Escola Politècnica Superior de Castelldefels
UNIVERSITAT POLITÈCNICA DE CATALUNYA

Microwave directional couplers

TITLE: Microwave directional couplers

MASTER DEGREE: Master in Science in Telecommunication Engineering & Management

AUTHOR: Carlos Sánchez Sierra

DIRECTOR: Daniele Modotto

DATE: July 19 th 2010

The project **"Microwave directional couplers"** was realized under the supervisor **Daniele Modotto**, assistant professor of the Department of Information Engineering, **University of Brescia.**

The university was founded in 1982 and is branched in 4 Faculties: The Faculty of Economics, The Faculty of Law, The Faculty of Engineering and The Faculty of Medicine and Surgery.

One of the most important departments of the Faculty of Engineering, "Ingegneria dell ´Informazione" in the years, has consolidated its role and image as a unique environment for conducting studies and research for Information and Communication Technologies (ICT) in a multi- disciplinary and inter-disciplinary fashion. This is why it is now called "Department of Information Engineering: Electronics, Informatics, Telecommunications and Control Systems" (DII).

Overview

This document contains the study of “Microwave directional couplers”.

Initiating with a waveguiding system, we are looking for solutions of Maxwell’s equations, then we focus on the TEM Transmission Lines and we introduce the microstrip lines that are used to convey microwave-frequency signals. It consists of a conducting strip separated from a ground plane by a dielectric layer known as the substrate. In this chapter one, we also solve the equations, and discuss their solutions, describing coupled lines.

In the second chapter, coupled microstrip lines are discussed. The configuration for these lines is shown in the document. We see the most important parameters that characterise a coupled microstrip line. Some of the important techniques for analyzing coupled lines are outlined. Coupled mode formulation and the even- and odd-mode method are described.

In the last chapter we realize series of simulations of coupled microstrip lines with the CST STUDIO SUITE™, program that allows us to make a more closely study. We can see how at the introduction of a transmission line more close to the other it is produced the coupling effect, transmitting the power with a proportion related with the fixed parameters that have been chosen.

In the final of the paper we present the conclusions of all the simulations that have been realized and we expose the most representative ones in the annexes.

INDEX

INTRODUCTION

The directional couplers are circuits that are essential in many optical communications systems and microwave bands. A directional couples is a device capable of extracting a part of a signal that travels over a transmission line or waveguide, leaving the rest of power not coupled direct route at the exit. Between its main applications we can mention the measurement of the power, the measurement of the stationary wave, sampling of the control signal, the combination of the microwave signals… They can even be used for performing signal processing tasks: part of balanced amplifiers, mixers, phase shifters, modulators, demodulators... .

We will study the “Microwave directional couplers”, with some variations.

In the first chapter, initiating with the waveguiding system, we are seeking solutions of Maxwell’s equations. Maxwell's equations are a set of four partial differential equations that relate the electric and magnetic fields to their sources, charge density and current density. These equations can be combined to show that light is an electromagnetic wave. For introducing the microstrip lines that are used to convey microwave-frequency signals, we first have to study the TEM Transmission Lines. It consists of a conducting strip separated from a ground plane by a dielectric layer known as the substrate. In the first chapter, we will also solve the equations, and discuss their solutions, describing coupled lines. We will realize a representation of the mathematically obtained equations in MatLab.

The next chapter, discuses coupled microstrip lines, whose configuration is shown in the paper. The more important parameters that characterize the coupled microstrip lines and also some of the main techniques for analyzing coupled lines are draft. We will also describe the coupled mode formulation and the even- and odd-mode method.

The last chapter brings in the simulations of the microstrip lines. These were realized with the CST STUDIO SUITE™ program, a program considered to be appropriate for a detailed study. We will see the coupling effect that is produced by introducing a line more close with the other. It can be observed the proportional transfer of the power related with the fixed chosen parameters.

The thesis will end with the conclusion of the simulations and with the annexes that present the main simulations results.

CHAPTER 1. COUPLED LINES

1.1. Waveguides

Waveguides are used to transfer electromagnetic power efficiently from one point in space to another. Some common guiding structures are the typical coaxial cable, the two-wire and mictrostrip transmission lines, hollow conducting waveguides, and optical fibers. In practice, the choice of structure is dictated by: the desired operating frequency band, the amount of power to be transferred, and the amount of transmission losses that can be tolerated.

Microstrip lines are used widely in microwave integrated circuits.

In a waveguiding system, we are looking for solutions of Maxwell's equations (look [1]) that are propagating along the guiding direction (the z direction) and are confined in the near vicinity of the guiding structure. Thus, the electric and magnetic fields are assumed to have the form:

$$\begin{aligned} E(x,y,z,t) &= E(x,y)e^{j\omega t - j\beta z} \\ H(x,y,z,t) &= H(x,y)e^{j\omega t - j\beta z} \end{aligned} \qquad \textbf{(1.1)}$$

where β is the propagation wavenumber along the guide direction. The corresponding wavelength, called the guide wavelength, is denoted by $\lambda_g = 2\pi/\beta$.

1.2. Transmission Lines

A transmission line is the material medium or structure that forms all or part of a path from one place to another for directing the transmission of energy, such as electromagnetic waves.

1.2.1. Properties of TEM Transmission Lines

In TEM modes, both E_z and H_z vanish, and the fields are fully transverse.

One can set $E_z = H_z = 0$ in Maxwell equations, the latter being equivalent to a two-dimensional electrostratic problem:

$$H_T = \frac{1}{\eta}\hat{z} \times E_T$$
$$\nabla_T \times E_T = 0$$
$$\nabla_T \cdot E_T = 0 \qquad \textbf{(1.2)}$$

The first of (1.2) are the electric and magnetic fields satisfy. Others are recognized as the field equations of an equivalent two-dimensional electrostatic problem. Thus, the electric field can be obtained from equivalent electrostatic problem:

$$\nabla_T^2 \varphi = 0$$
$$E_T = -\nabla_T \varphi \qquad \textbf{(1.3)}$$

Because in electrostatic problems the electric field lines must start at positively charged conductors and end at negatively charged ones, a TEM mode can be supported only in multi-conductor guides. Fig. 1.1 depicts the transverse cross-sectional area of a two-conductor transmission line. The cross-section shapes are arbitrary.

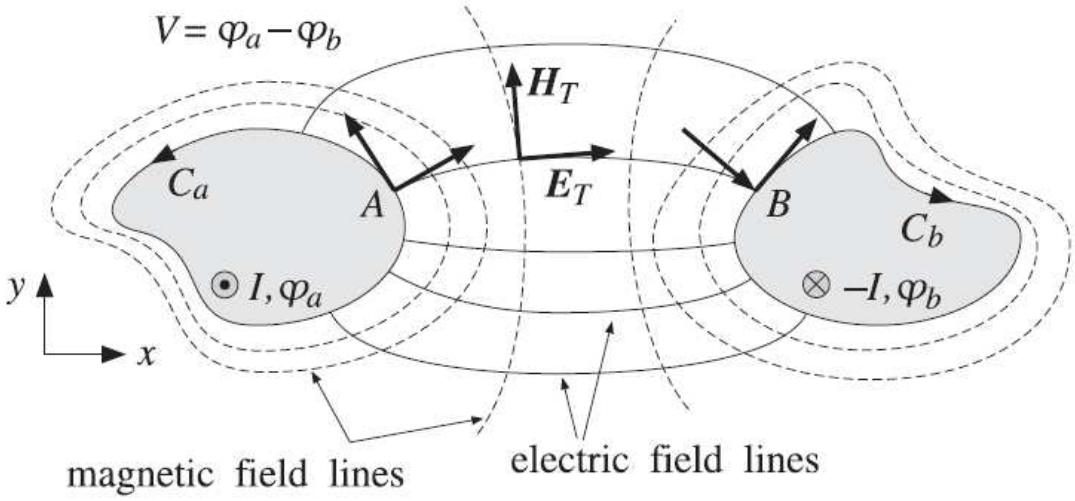

Fig. 1.1 Two-conductor transmission line.

The conductors are equipotentials of the electrostatic solution. Let φ_a, φ_b be the constant potentials on the two conductors. The voltage difference between the conductors will be $V = \varphi a - \varphi b$. The electric field lines start perpendicularly on conductor (a) and end perpendicularly on conductor (b). The magnetic field lines, being perpendicular to the electric lines according to equation (1.2), are

recognized to be the equipotential lines. As such, they close upon themselves surrounding the two conductors. In particular, on the conductor surfaces the magnetic field is tangential. According to Ampere's law, the line integrals of the magnetic field around each conductor will result into total currents I and $-I$ flowing on the conductors in the z-direction. These currents are equal and opposite.

1.2.2. Microstrip Lines

Microstrip is a type of electrical transmission line which can be fabricated using printed circuit board [PCB] technology, and is used to convey microwave-frequency signals. It consists of a conducting strip separated from a ground plane by a dielectric layer known as the substrate.

Practical microstrip lines, shown in Fig. 1.2, have width-to-height ratios w/h that are not necessarily much greater than unity, and can vary over the interval 0.1 < w/h < 10. Typical heights h are of the order of millimeters.

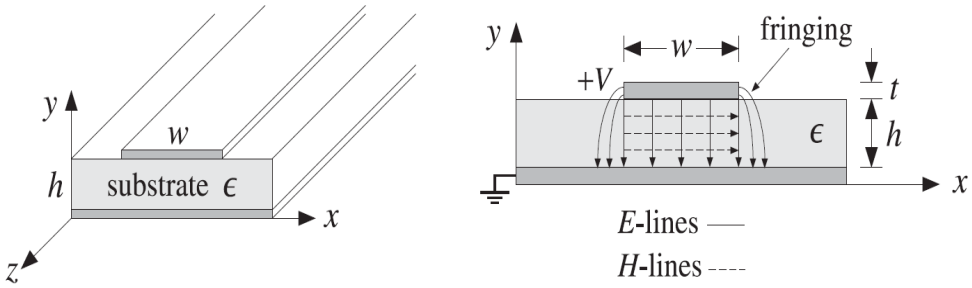

Fig. 1.2 A microstrip transmission line.

Fringing effects cannot be ignored completely and the simple assumptions about the fields of the parallel plate line are not valid. For example, assuming a propagating wave in the z-direction with z, t, dependence of $e^{j\omega t - j\beta z}$ with a common β in the dielectric and air, the longitudinal-transverse decomposition gives:

$$\hat{z} \times (\nabla_T E_Z + j\beta E_T) = j\omega\mu H_T \qquad \textbf{(1.4)}$$

In particular, the air-dielectric interface is replaced by an effective dielectric, filling uniformly the entire space, and in which there would be a TEM propagating mode. If we denote by eff the relative permittivity of the effective dielectric, the wavelength and velocity factor of the line will be given in terms of their free-space values λ_0, c_0:

$$\lambda=\frac{\lambda_0}{\sqrt{\epsilon_{eff}}} \quad , \quad c=\frac{c_0}{\sqrt{\epsilon_{eff}}} \tag{1.5}$$

There exist many empirical formulas for the characteristic impedance of the line and the effective dielectric constant.

Some typical substrate dielectric materials used in microstrip lines are alumina, a ceramic form of Al_2O_4 with $\epsilon_r=9.8$, and RT-Duroid, a Teflon composite material with $\epsilon_r=2.2$.

The synthesis of a microstrip line requires that we determine the ratio w/h that will achieve a given characteristic impedance Z. Practical values of characteristic impedances are between 10–200 ohm.

1.3. Coupled Transmission Lines

Coupling between two transmission lines is introduced by their proximity to each other.

Coupling effects may be undesirable, such as crosstalk in printed circuits, or they may be desirable, as in directional couplers where the objective is to transfer power from one line to the other.

In this sections, we solve the equations, and discuss their solutions, describing coupled lines. Fig. 1.3 shows an example of two coupled microstrip lines over a common ground plane, and also shows a generic circuit model for coupled lines.

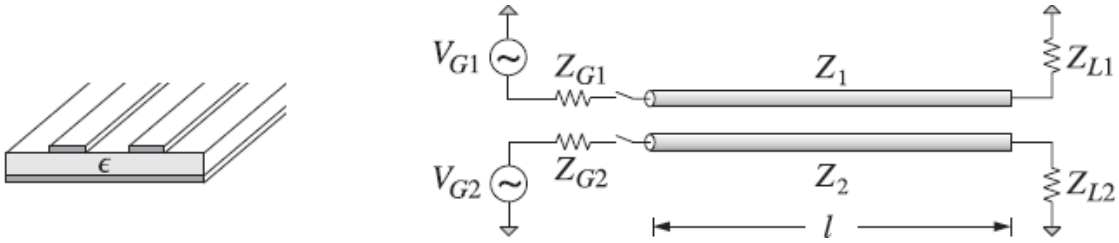

Fig. 1.3 Coupled Transmission Lines.

For simplicity, we assume that the lines are lossless. Let $L_i, C_i \quad i=1,2$ be the distributed inductances and capacitances per unit length when the lines are isolated from each other. The corresponding propagation velocities and characteristic impedances are: $v_i=1/\sqrt{L_i C_i}$, $Z_i=\sqrt{L_i/C_i}$, $i=1,2$. C_1 is related to the capacitance to ground C_{1g} via $C_1=C_{1g}+C_m$, so that the total charge per unit length on line-1 is $Q_1=C_1V_1-C_mV_2=C_{1g}(V_1-V_g)+C_m(V_1-V_2)$, where $V_g=0$. The coupling between the lines is modeled by introducing a mutual

inductance and capacitance per unit length, L_m, C_m. Then, the coupled versions of telegrapher's equations become:

$$\frac{\partial V_1}{\partial z} = -L_1\frac{\partial I_1}{\partial t} - L_m\frac{\partial I_2}{\partial t} \quad , \quad \frac{\partial I_1}{\partial z} = -C_1\frac{\partial V_1}{\partial t} + C_m\frac{\partial V_2}{\partial t}$$
$$\frac{\partial V_2}{\partial z} = -L_2\frac{\partial I_2}{\partial t} - L_m\frac{\partial I_1}{\partial t} \quad , \quad \frac{\partial I_2}{\partial z} = -C_2\frac{\partial V_2}{\partial t} + C_m\frac{\partial V_1}{\partial t} \qquad \textbf{(1.6)}$$

When $L_m = C_m = 0$, they reduce to uncoupled equation describing the isolated individual lines. The equations (1.6) may be written in the 2x2 matrix form:

$$\frac{\partial V_1}{\partial z} = -\begin{bmatrix} L_1 & L_m \\ L_m & L_2 \end{bmatrix}\frac{\partial I_1}{\partial t}$$
$$\frac{\partial I_1}{\partial z} = -\begin{bmatrix} C_1 & -C_m \\ -C_m & C_2 \end{bmatrix}\frac{\partial V_1}{\partial t} \qquad \textbf{(1.7)}$$

where V,I are the column vectors:

$$V = \begin{bmatrix} V_1 \\ V_2 \end{bmatrix} \quad , \quad I = \begin{bmatrix} I_1 \\ I_2 \end{bmatrix} \qquad \textbf{(1.8)}$$

For sinusoidal time dependence $e^{j\omega t}$, the system (1.7) becomes:

$$\frac{dV_1}{dz} = -\begin{bmatrix} L_1 & L_m \\ L_m & L_2 \end{bmatrix} I$$
$$\frac{dI_1}{dz} = -\begin{bmatrix} C_1 & -C_m \\ -C_m & C_2 \end{bmatrix} V \qquad \textbf{(1.9)}$$

Electromagnetic Waves (look [1]), proves to be convenient to recast these equations in terms of the forward and backward waves that are normalized with respect to the uncoupled impedances Z_1, Z_2 :

$$a_1=\frac{V_1+Z_1 I_1}{\sqrt{2\,Z_1}} \quad , \quad b_1=\frac{V_1-Z_1 I_1}{\sqrt{2\,Z_1}}$$
$$a_2=\frac{V_2+Z_2 I_2}{\sqrt{2\,Z_2}} \quad , \quad b_2=\frac{V_2-Z_2 I_2}{\sqrt{2\,Z_2}} \rightarrow a=\begin{bmatrix} a_1 \\ a_2 \end{bmatrix} \quad , \quad b=\begin{bmatrix} b_1 \\ b_2 \end{bmatrix} \qquad \textbf{(1.10)}$$

The total average power on the line can be expressed conveniently in terms of these:

$$P=\frac{1}{2}\Re[V^{\dagger} I]=\frac{1}{2}\Re[V_1^{*} I_1]+\frac{1}{2}\Re[V_2^{*} I_2]=P_1+P_2$$
$$P=(|a_1|^2-|b_1|^2)+(|a_2|^2-|b_2|^2)=(|a_1|^2+|b_1|^2)-(|a_2|^2+|b_2|^2) \qquad \textbf{(1.11)}$$
$$P=a^{\dagger} a-b^{\dagger} b$$

where the dagger operator denotes the conjugate-transpose, for example, $a\dagger=[a_1^{*}, a_2^{*}]$.

Thus, the a-waves carry power forward, and the b-waves, backward. After some algebra, it can be shown that equation. (1.9) are equivalent to the system:

$$\boxed{\begin{aligned} \frac{da}{dz} &= -jFa+jGb \\ \frac{db}{dz} &= -jGa+jFb \end{aligned}} \rightarrow \frac{d}{dz}\begin{bmatrix} a \\ b \end{bmatrix}=-j\begin{bmatrix} F & -G \\ G & -F \end{bmatrix}\begin{bmatrix} a \\ b \end{bmatrix} \qquad \textbf{(1.12)}$$

with the matrices F, G given by:

$$F=\begin{bmatrix} \beta_1 & \kappa \\ \kappa & \beta_1 \end{bmatrix} \quad , \quad G=\begin{bmatrix} 0 & \chi \\ \chi & 0 \end{bmatrix} \qquad \textbf{(1.13)}$$

where β_1, β_2 are the uncoupled wavenumbers $\beta_i=\omega/v_i=\omega L_i C_i, i=1,2$ and the coupling parameters κ, χ are:

$$\kappa=\frac{1}{2}\omega\left(\frac{L_m}{\sqrt{Z_1 Z_2}}-C_m\sqrt{Z_1 Z_2}\right) = \frac{1}{2}\sqrt{\beta_1\beta_2}\left(\frac{L_m}{\sqrt{L_1 L_2}}-\frac{C_m}{\sqrt{C_1 C_2}}\right)$$
$$\chi=\frac{1}{2}\omega\left(\frac{L_m}{\sqrt{Z_1 Z_2}}+C_m\sqrt{Z_1 Z_2}\right) = \frac{1}{2}\sqrt{\beta_1\beta_2}\left(\frac{L_m}{\sqrt{L_1 L_2}}+\frac{C_m}{\sqrt{C_1 C_2}}\right) \quad \textbf{(1.14)}$$

A consequence of the structure of the matrices F, G is that the total power P defined in (1.11) is conserved along z.

For the design of our study, we specialize to the case of two identical lines that have $L_1=L_2\equiv L_0$ and $C_1=L_2\equiv L_0$, so that $\beta_1=\beta_2=\omega\ L_0C_0\equiv\beta$ and $Z_1=Z_2=L_0/C_0\equiv Z_0$, and speed $v_0=1/L_0C_0$. Then, the a, b waves and the matrices F, G take the simpler forms:

$$a=\frac{V+Z_0 I}{\sqrt{2\,Z_0}} \quad , \quad b=\frac{V-Z_0 I}{\sqrt{2\,Z_0}} \ \rightarrow\ a=\frac{V+Z_0 I}{2} \quad , \quad b=\frac{V-Z_0 I}{2} \quad \textbf{(1.15)}$$

$$F=\begin{bmatrix}\beta & \kappa\\ \kappa & \beta\end{bmatrix} \ , \quad G=\begin{bmatrix}0 & \chi\\ \chi & 0\end{bmatrix} \quad \textbf{(1.16)}$$

where for simplicity, we removed the common scale factor $\sqrt{2\,Z_0}$ from the denominator of a, b. The coupling parameters κ, χ are obtained by setting $Z_1=Z_2=Z_0$ in (1.14):

$$\kappa= \frac{1}{2}\beta\left(\frac{L_m}{L_0}-\frac{C_m}{C_0}\right) \quad , \quad \chi= \frac{1}{2}\beta\left(\frac{L_m}{L_0}+\frac{C_m}{C_0}\right) \quad \textbf{(1.17)}$$

As is showed in Electromagnetic Waves (look [1]), this system can be decoupled by forming the following linear combinations of the a, b waves:

$$\begin{matrix}A=a-\Gamma b\\ B=b-\Gamma a\end{matrix} \rightarrow \begin{bmatrix}A\\ B\end{bmatrix}=\begin{bmatrix}I & -\Gamma\\ -\Gamma & I\end{bmatrix}\begin{bmatrix}a\\ b\end{bmatrix} \quad \textbf{(1.18)}$$

The A, B can be written in terms of V, I and the impedance matrix Z as follows:

$$\begin{aligned} A &= (2\mathrm{D})^{-1}(V+ZI) \\ B &= (2\mathrm{D})^{-1}(V-ZI) \end{aligned} \quad \rightarrow \quad \begin{aligned} V &= D(A+B) \\ ZI &= D(A-B) \end{aligned} \qquad D = \frac{Z+Z_0 I}{2Z_0} \qquad \textbf{(1.19)}$$

Using (1.18), we obtain the solutions for V, I expressed in terms of the matrix exponentials $e^{\pm j\mathcal{B}z}$, where $\mathcal{B} = \sqrt{(F+G)(F-G)}$

$$\begin{aligned} V(z) &= D\left[e^{-j\mathcal{B}z}A(0) + e^{j\mathcal{B}z}B(0)\right] \\ ZI(z) &= D\left[e^{-j\mathcal{B}z}A(0) - e^{j\mathcal{B}z}B(0)\right] \end{aligned} \qquad \textbf{(1.20)}$$

To be able to understand, to represent and to complete the solution, we terminate both lines at common generator and load impedances, that is, $Z_{G1} = Z_{G2} \equiv Z_G$ and $Z_{L1} = Z_{L2} \equiv Z_L$. The generator voltages V_{G1}, V_{G2} are assumed to be different. We define the generator voltage vector and source and load matrix reflection coefficients:

$$V_G = \begin{bmatrix} V_{G1} \\ V_{G2} \end{bmatrix} \quad , \qquad \begin{aligned} \Gamma_G &= (Z_G I - Z)(Z_G I + Z)^{-1} \\ \Gamma_L &= (Z_L I - Z)(Z_L I + Z)^{-1} \end{aligned} \qquad \textbf{(1.21)}$$

The terminal conditions for the line are at $z = 0$ and $z = l$:

$$V_G = V(0) + Z_G I(0) \quad , \quad V(l) = Z_L I(l) \qquad \textbf{(1.22)}$$

They may be re-expressed in terms of A, B with the help of (1.19):

$$A(0) - \Gamma_G B(0) = D^{-1} Z (Z + Z_G I)^{-1} V_G \quad , \quad B(l) = \Gamma_L A(l) \qquad \textbf{(1.23)}$$

but expressed in terms of the matrix exponentials, we have:

$$e^{j\mathcal{B}l} B(0) = B(l) = \Gamma_L A(l) = \Gamma_L e^{-j\mathcal{B}l} A(0) \quad \rightarrow \quad B(0) = \Gamma_L e^{-2j\mathcal{B}l} A(0) \qquad \textbf{(1.24)}$$

Inserting this into (1.23), we may solve for $A(0)$ in terms of the generator voltage:

$$A(0)=D^{-1}[I-\Gamma_G\Gamma_L e^{-2j\beta l}]^{-1}Z(Z+Z_G I)^{-1}V_G \qquad \textbf{(1.25)}$$

Using (1.25) into (1.20), we finally obtain the voltage and current at an arbitrary position z along the lines:

$$\boxed{\begin{aligned} V(z)&=[e^{-j\beta z}+\Gamma_L e^{-2j\beta l}e^{j\beta z}][I-\Gamma_G\Gamma_L e^{-2j\beta l}]^{-1}Z(Z+Z_G I)^{-1}V_G \\ I(z)&=[e^{-j\beta z}-\Gamma_L e^{-2j\beta l}e^{j\beta z}][I-\Gamma_G\Gamma_L e^{-2j\beta l}]^{-1}(Z+Z_G I)^{-1}V_G \end{aligned}} \qquad \textbf{(1.26)}$$

Resolving V_G and $V(z)$ into their even and odd modes, that is, expressing them as linear combinations of the eigenvectors $e_\pm=\frac{1}{\sqrt{2}}\begin{bmatrix}1\\ \mp 1\end{bmatrix}$, we have:

$$\begin{aligned} V_G&=V_{G+}e_+ + V_{G-}e_- \quad , \quad where \quad V_{G\pm}=\frac{V_{G1}\pm V_{G2}}{\sqrt{2}} \\ V(z)&=V_+(z)e_+ + V_-(z)e_- \quad , \quad V_\pm(z)=\frac{V_1(z)\pm V_2(z)}{\sqrt{2}} \end{aligned} \qquad \textbf{(1.27)}$$

In this basis, the matrices in (1.26) are diagonal resulting in the equivalent solution:

$$\begin{aligned} V(z)=V_+(z)e_+ + V_-(z)e_- = &\frac{e^{-j\beta_+ z}+\Gamma_{L+}e^{-2j\beta_+ l}e^{j\beta_+ z}}{1-\Gamma_{G+}\Gamma_{L+}e^{-2j\beta_+ l}}\frac{Z_+}{Z_+ + Z_G}V_{G+}e_+ \\ &+\frac{e^{-j\beta_- z}+\Gamma_{L-}e^{-2j\beta_- l}e^{j\beta_- z}}{1-\Gamma_{G-}\Gamma_{L-}e^{-2j\beta_- l}}\frac{Z_-}{Z_- + Z_G}V_{G-}e_- \end{aligned} \qquad \textbf{(1.28)}$$

where $\beta_\pm$ are the eigenvalues of B, $Z_\pm$ the eigenvalues of Z, and $\Gamma_{G\pm}, \Gamma_{L\pm}$ are:

$$\Gamma_{G\pm}=\frac{Z_G - Z_\pm}{Z_G + Z_\pm} \quad , \quad \Gamma_{L\pm}=\frac{Z_L - Z_\pm}{Z_L + Z_\pm} \qquad \textbf{(1.29)}$$

The voltages $V_1(z), V_2(z)$ are obtained by extracting the top and bottom components of (1.28), that is, $V_{1,2}(z)=[V_+(z)\pm V_-(z)]/\sqrt{2}$:

$$V_1(z)=\frac{e^{-j\beta_+ z}+\Gamma_{L+}e^{-2j\beta_+ l}e^{j\beta_+ z}}{1-\Gamma_{G+}\Gamma_{L+}e^{-2j\beta_+ l}}V_+ +\frac{e^{-j\beta_- z}+\Gamma_{L-}e^{-2j\beta_- l}e^{j\beta_- z}}{1-\Gamma_{G-}\Gamma_{L-}e^{-2j\beta_- l}}V_-$$

$$V_2(z)=\frac{e^{-j\beta_+ z}+\Gamma_{L+}e^{-2j\beta_+ l}e^{j\beta_+ z}}{1-\Gamma_{G+}\Gamma_{L+}e^{-2j\beta_+ l}}V_+ -\frac{e^{-j\beta_- z}+\Gamma_{L-}e^{-2j\beta_- l}e^{j\beta_- z}}{1-\Gamma_{G-}\Gamma_{L-}e^{-2j\beta_- l}}V_- \qquad \textbf{(1.30)}$$

where we defined:

$$V_\pm=\left(\frac{Z_\pm}{Z_\pm+Z_G}\right)\frac{V_{G\pm}}{\sqrt{2}}=\frac{1}{4}(1-\Gamma_{G\pm})(V_{G1}\pm V_{G2}) \qquad \textbf{(1.31)}$$

The parameters $\beta_\pm, Z_\pm$ are obtained using the diagonalization rules. From equation (1.14), we find the eigenvalues of the matrices $F\pm G$:

$$(F+G)_\pm=\beta_\pm(\kappa+\chi)=\beta(1\pm\frac{L_m}{L_0})=\omega\frac{1}{Z_0}(L_0\pm L_m)$$

$$(F-G)_\pm=\beta_\pm(\kappa-\chi)=\beta(1\mp\frac{C_m}{C_0})=\omega\frac{1}{Z_0}(C_0\mp C_m) \qquad \textbf{(1.32)}$$

Then, it follows that:

$$\beta_+=\sqrt{(F+G)_+(F-G)_+}=\omega\sqrt{(L_0+L_m)(C_0-C_m)}$$

$$\beta_-=\sqrt{(F+G)_-(F-G)_-}=\omega\sqrt{(L_0-L_m)(C_0+C_m)} \qquad \textbf{(1.33)}$$

$$Z_+=Z_0\sqrt{\frac{(F+G)_+}{(F-G)_+}}=\sqrt{\frac{L_0+L_m}{C_0-C_m}}$$

$$Z_-=Z_0\sqrt{\frac{(F+G)_-}{(F-G)_-}}=\sqrt{\frac{L_0-L_m}{C_0+C_m}} \qquad \textbf{(1.34)}$$

Thus, the coupled system acts as two uncoupled lines with wavenumbers and characteristic impedances $\beta_\pm, Z_\pm$, propagation speeds $v_\pm=1/(L_0\pm L_m)(C_0\mp C_m)$, and propagation delays $T_\pm=l/v_\pm$. The even mode is energized when $V_{G2}=V_{G1}$, or, $V_{G+}\neq 0,\ V_{G-}=0$, and the odd mode, when $V_{G2}=-V_{G1}$, or, $V_{G+}=0,\ V_{G-}\neq 0$.

We can observe that these solutions following the most general solution form of the coupled system. It is expressible as a sum of a forward and a backward moving wave:

$$V(z)=V_+e^{-j\beta z}+V_-e^{j\beta z}=V_+(z)+V_-(z)$$
$$I(z)=\frac{1}{Z}V_+e^{-j\beta z}-V_-e^{j\beta z}=\frac{1}{Z}V_+(z)-V_-(z) \qquad \textbf{(1.35)}$$

Another equivalent solution of the currents $I_1(z), I_2(z)$, as we did with the voltage, is obtained from the matrix (1.26), by having studied the most general solution form of the coupled system (1.35).

$$I_1(z)=\frac{e^{-j\beta_+ z}-\Gamma_{L+}e^{-2j\beta_+ l}e^{j\beta_+ z}}{1-\Gamma_{G+}\Gamma_{L+}e^{-2j\beta_+ l}}\frac{V_+}{Z_+}+\frac{e^{-j\beta_- z}-\Gamma_{L-}e^{-2j\beta_- l}e^{j\beta_- z}}{1-\Gamma_{G-}\Gamma_{L-}e^{-2j\beta_- l}}\frac{V_-}{Z_-}$$
$$I_2(z)=\frac{e^{-j\beta_+ z}-\Gamma_{L+}e^{-2j\beta_+ l}e^{j\beta_+ z}}{1-\Gamma_{G+}\Gamma_{L+}e^{-2j\beta_+ l}}\frac{V_+}{Z_+}-\frac{e^{-j\beta_- z}-\Gamma_{L-}e^{-2j\beta_- l}e^{j\beta_- z}}{1-\Gamma_{G-}\Gamma_{L-}e^{-2j\beta_- l}}\frac{V_-}{Z_-} \qquad \textbf{(1.36)}$$

1.4. Matlab representation of two coupled microstrip lines

In this part, we represent the coupled microstrip lines system, Fig. 1.3, in MatLab with the equations obtained previously.

MatLab is able to calculate the time evolution of systems of ordinary differential equations of first order, linear and nonlinear. All solvers solve systems of equations in the form $y=f(y,t)$.

To transform the equations (1.12) to the desired form, we have to make some changes:

$$\begin{aligned}\frac{da}{dz}&=-jFa+jGb\\ \frac{db}{dz}&=-jGa+jFb\end{aligned}\rightarrow\ \frac{d}{dz}\begin{bmatrix}a\\b\end{bmatrix}=-j\begin{bmatrix}F&-G\\G&-F\end{bmatrix}\begin{bmatrix}a\\b\end{bmatrix} \qquad \textbf{(1.12)}$$

Where $a=\begin{bmatrix}a_1\\a_2\end{bmatrix}$, $b=\begin{bmatrix}b_1\\b_2\end{bmatrix}$ and using the definition of the matrices F, G , equations (1.16). We obtain a equivalent solution:

$$\frac{d}{dz}\begin{bmatrix} a_1 \\ a_2 \end{bmatrix} = -j\begin{bmatrix} \beta & \kappa \\ \kappa & \beta \end{bmatrix}\begin{bmatrix} a_1 \\ a_2 \end{bmatrix} + j\begin{bmatrix} 0 & \chi \\ \chi & 0 \end{bmatrix}\begin{bmatrix} b_1 \\ b_2 \end{bmatrix}$$
$$\frac{d}{dz}\begin{bmatrix} b_1 \\ b_2 \end{bmatrix} = -j\begin{bmatrix} 0 & \chi \\ \chi & 0 \end{bmatrix}\begin{bmatrix} a_1 \\ a_2 \end{bmatrix} + j\begin{bmatrix} \beta & \kappa \\ \kappa & \beta \end{bmatrix}\begin{bmatrix} b_1 \\ b_2 \end{bmatrix} \quad \textbf{(1.37)}$$

Changing the equation form, it results this:

$$\frac{d}{dz}a_1 = -j(\beta a_1 + \kappa a_2) + j\chi b_2$$
$$\frac{d}{dz}a_2 = -j(\kappa a_1 + \beta a_2) + j\chi b_1$$
$$\frac{d}{dz}b_1 = -j\chi a_2 + j(\beta b_1 + \kappa b_2) \quad \textbf{(1.38)}$$
$$\frac{d}{dz}b_2 = -j\chi a_1 + j(\kappa b_1 + \beta b_2)$$

MatLab has several features to integrate systems of ordinary differential equations of first order, including ode23, which uses the Runge-Kutta method of second-third order. It requires the user to write a function to compute the derivatives from the vector of variables.

The ode23 does not allow complex variable. Then, the solution is to convert a system of four complex variables in a system of eight real variables with the following change:

$$\begin{aligned} a_1 &= a_{1R} + j\,a_{1I} \\ a_2 &= a_{2R} + j\,a_{2I} \\ b_1 &= b_{1R} + j\,b_{1I} \\ b_2 &= b_{2R} + j\,b_{2I} \end{aligned} \quad \rightarrow \quad \begin{aligned} \frac{d}{dz}a_1 &= \frac{d}{dz}a_{1R} + j\frac{d}{dz}a_{1I} \\ \frac{d}{dz}a_2 &= \frac{d}{dz}a_{2R} + j\frac{d}{dz}a_{2I} \\ \frac{d}{dz}b_1 &= \frac{d}{dz}b_{1R} + j\frac{d}{dz}b_{1I} \\ \frac{d}{dz}b_2 &= \frac{d}{dz}b_{2R} + j\frac{d}{dz}b_{2I} \end{aligned} \quad \textbf{(1.39)}$$

Inserting the equations (1.39) into the equivalent solution of the coupled microstrip lines system without matrices, equations (1.38), we obtain another equivalent system with eight real variables and simple equations:

$$\begin{aligned}
\frac{d}{dz}a_{1R} &= \beta a_{1I} + \kappa a_{2I} - \chi b_{2I} & \frac{d}{dz}b_{1R} &= -\beta b_{1I} - \kappa b_{2I} + \chi a_{2I} \\
\frac{d}{dz}a_{1I} &= \chi b_{2R} - \beta a_{1R} - \kappa a_{2R} & \frac{d}{dz}b_{1I} &= -\chi a_{2R} + \beta b_{1R} + \kappa b_{2R} \\
\frac{d}{dz}a_{2R} &= \kappa a_{1I} + \beta a_{2I} - \chi b_{1I} & \frac{d}{dz}b_{2R} &= -\kappa b_{1I} - \beta b_{2I} + \chi a_{1I} \\
\frac{d}{dz}a_{2I} &= \chi b_{1R} - \kappa a_{1R} - \beta a_{2R} & \frac{d}{dz}b_{2I} &= -\chi a_{1R} + \kappa b_{1R} + \beta b_{2R}
\end{aligned} \qquad \textbf{(1.40)}$$

The most basic way for all MatLab integrators is:

$$[T, Y] = solvername(fh, tspan, y0) \qquad \textbf{(1.41)}$$

where fh is a reference to the function that calculates the derivative according to the expression ($y = f(y,t)$), $tspan$ can be a vector of two elements $[tini, tfinal]$ that represent the beginning and the end of integration or a vector of times $[tini:tstep:tfinal]$ in which you want MatLab to return results, and $y0$ is a column vector with initial values. The result is T, the times vector where results are given and a matrix Y with as many rows as times of exit and to represent each exit in the corresponding instant of time.

We can see in (Annex 1), the MatLab code used for the following example, Fig. 1.4, with all its functions and subfunctions.

For the following examples we choose: The dielectric material is copper, which has the effective dielectric constant $\epsilon_r = 4{,}7$ and $L_m/L_0 = 0{,}4 \quad C_m/C_0 = 0{,}3$. The uncoupled line impedance was $Z_0 = 50\,\Omega$. The intrinsic conductance C_0 and inductance L_0 can be found in the following equations:

$$\begin{aligned}
L_0 &= Z_0 33{,}36\sqrt{0{,}475\epsilon_r + 0{,}67} \times 10^{-3} \quad [nH/cm] \\
C_0 &= \frac{33{,}36\sqrt{0{,}475\epsilon_r + 0{,}67}}{z_0} \quad [pF/cm]
\end{aligned} \qquad \textbf{(1.42)}$$

Fig. 1.4 shows the signals $a_1(z)$, $a_2(z)$, $b_1(z)$, $b_2(z)$ for a pair of coupled lines using the MatLab integrator (ode23).

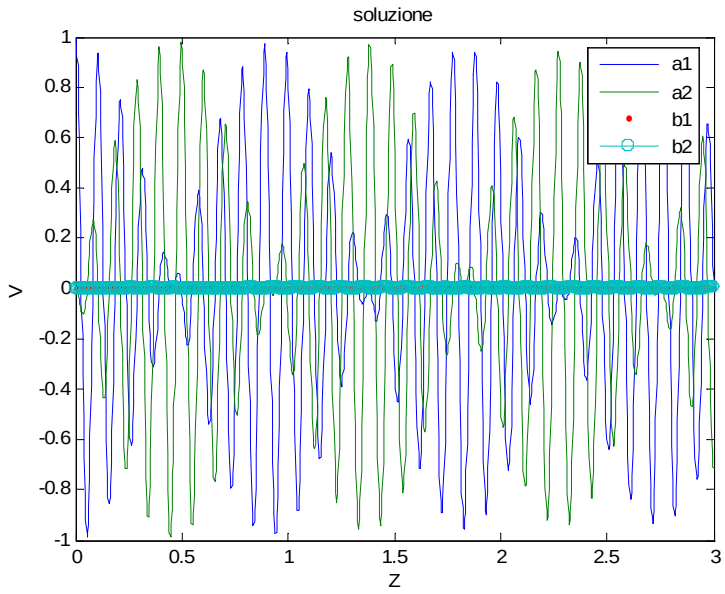

Fig. 1.4 The a-waves carry power forward, and the b-waves, backward.

Getting a signal just input a_1=1 the Fig.1.4 shows how the signal is transmitted from one line to another and back (a_1 , a_2). We can also see that the reflected wave of each line is practically none (b_1 , b_2).

To further explore the theory of coupled lines and make the verification of previous system, now we represent directly in MatLab the theoretical solution (1.30) of the differential equation (1.12) of coupled transmission lines.

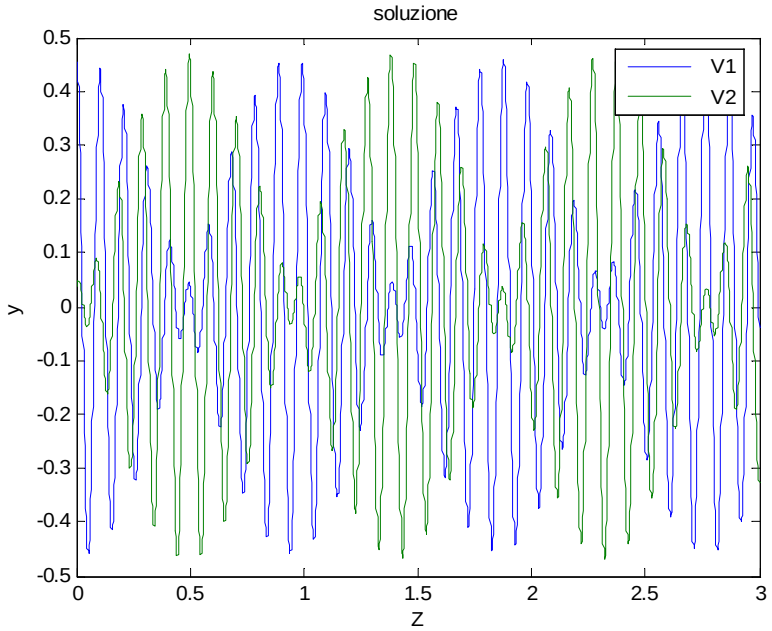

Fig. 1.5 Signals along the coupled lines.

We can see in (Annex 2), the MatLab code used in this example, Fig. 1.5, with all its functions.

The generator voltages are assumed to be different, one active and the other off, $V_{G1}=1$ and $V_{G2}=0$. We see the same effect of power transmission between two coupled lines due to having introduced the same line characteristics $\epsilon_r, L_m, L_0, C_m, C_0, Z_0$, in both examples, but it is not exactly the same graphics, there is a difference of amplitude between the two systems due to the differences entries, initial values.

The equations (1.10) relate the two systems, the theoretical solution (1.30) and the differential equation (1.12) of coupled transmission lines:

$$a_i=\frac{V_i+Z_0 I_i}{\sqrt{2\,Z_0}} \quad , \quad b_i=\frac{V_i-Z_0 I_i}{\sqrt{2\,Z_0}} \quad \rightarrow \quad \begin{matrix} V_i=(a_i+b_i)\frac{\sqrt{Z_0}}{\sqrt{2}} \\ I_i=(a_i-b_i)\frac{1}{\sqrt{2Z_0}} \end{matrix} \qquad \textbf{(1.43)}$$

$$where: i=(1,2)$$

If a generator voltages is active and the other off, $V_{G1}=1$ and $V_{G2}=0$, we find the initial values $(a_i(0), b_i(0))$ the differential equation system as follows:

The equations (1.31) define the parameters $V_{\pm'}$ of the system (1.30) and (1.36) to found the initial values of voltage and current ($V_i(0), I_i(0)$) . Thus, again using the equation (1.10) or (1.43) with initial values for voltage and current ($V_i(0), I_i(0)$), we find the initial values of $(a_i(0), b_i(0))$ to have the same input in both systems.

$$a_i(0)=\frac{V_i(0)+Z_0 I_i(0)}{\sqrt{2\,Z_0}} \quad , \quad b_i(0)=\frac{V_i(0)-Z_0 I_i(0)}{\sqrt{2\,Z_0}} \qquad \textbf{(1.43)}$$

$$where: i=(1,2)$$

The next figure, Fig. 1.6, shows the signals $V_1(z)$, $V_2(z)$ for a pair of coupled lines, used MatLab integrator (ode23), with the initial values $(a_i(0), b_i(0))$ previously calculated.

We can see in (Annex 3), the MatLab code used for the following example, Fig. 1.6, with all its functions and subfunctions performing this change of variables and compare it with theoretical solution.

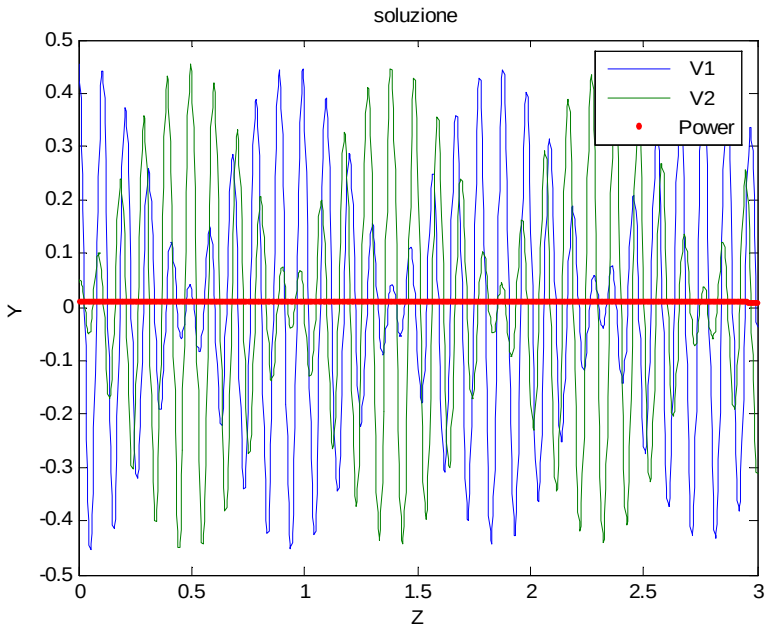

Fig. 1.6 Signals and power along the coupled lines.

Fig.1.5 and Fig1.6 figures are exactly the same, with the same frequency and amplitude, possibly with a negligible error due to Matlab's own error.

The red line in the graph, Fig1.6, shows the total average power in the line. The total power P defined in equation (1.11) is conserved along z, by assuming a system without losses.

With all these data seen so far, we have studied the mathematical theoretical functioning of the systems of two coupled transmission lines.

CHAPTER 2. DIRECTIONAL COUPLERS

The directional couplers are passive devices used in the field of radio technology. These devices fit of the power transmitted through a transmission line to another port using two transmission lines placed close enough so that the energy flowing through one of the lines are coupled to each other.

Directional couplers are defined to be passive microwave components used for power division. We say that an RF component is passive, if it does not require any power or energy to function properly. For a better understanding and to get a clearer image of these two passive microwave components we are using Figure 2.1. During the whole process of power division we can notice that the four-port networks take the form of directional couplers and hybrids. While directional couplers can be created having in mind the arbitrary power division, the hybrid junctions have frequently identical power division. Regarding the hybrid junctions we can take in consideration two situations: a 90° (quadrate) or a 180° (magic-T) phase shift between the outport po rts.

Looking back at the important steps that have been taken in the history, is important to mention that at the MIT Radiation Laboratory in the 1940s, were invented and characterized a diversity of waveguide couplers, including E- and H-plane waveguide tee junctions, the Bethe hole coupler, multihole directional couplers, the Schwinger coupler, the waveguide magic-T, and several types of couplers using coaxial probes. Another important phase in development of the couplers is the period between 1950s and 1960s, when it took place a reinvention of a lot of them to use stripline or microstrip technology. New types of couplers, like the branch line hybrid, and the coupled line directional coupler also had benefit of a development, due to the expanding use of planar lines.

In this chapter, will start with a presentation of the general properties of four-port networks, and we will continue with the analyse, the design and the simulation of the couplers.

2.1 Basic Properties

2.1.1 Four-Port Networks

The S matrix of the reciprocal and mathed four-port network has the following form:

$$[S]=\begin{bmatrix} 0 & S_{12} & S_{13} & S_{14} \\ S_{12} & 0 & S_{23} & S_{24} \\ S_{13} & S_{23} & 0 & S_{34} \\ S_{14} & S_{24} & S_{34} & 0 \end{bmatrix} \qquad \textbf{(2.1)}$$

If the network is matched at every port, then $S_{11}=S_{22}=S_{33}=S_{44}=0$. (It is important to understand that "matched" means $\Gamma_1, \Gamma_2, \Gamma_3$ and $\Gamma_4=0$ when all other ports are terminated in Z_0).

If the network is reciprocal, then $S_{21}=S_{12}$, $S_{31}=S_{13}$, $S_{32}=S_{23}$, $S_{41}=S_{14}$, $S_{42}=S_{24}$, $S_{43}=S_{34}$.

Incorporating the fact that the network is lossless puts further constraints on these S parameters, 10 equations result from the unitarity, or energy conservation. Let us consider the multiplication of row 1 and row 2, and the multiplication of row 4 and row 3, also similarly, the multiplication of row 1 and row 3, and the multiplication of row 4 and row 2, give:

$$\begin{aligned} S_{13}^{*}S_{23}+S_{14}^{*}S_{24}&=0 \\ S_{14}^{*}S_{13}+S_{24}^{*}S_{23}&=0 \\ S_{12}^{*}S_{23}+S_{14}^{*}S_{34}&=0 \\ S_{14}^{*}S_{12}+S_{34}^{*}S_{23}&=0 \end{aligned} \qquad \textbf{(2.2)}$$

Now multiply (2.2) the first equation by S_{24}^{*}, the second by S_{13}^{*}, the third by S_{12} and the fourth by S_{34}, and subtract to obtain:

$$\begin{aligned} S_{14}^{*}(|S_{13}|^2-|S_{24}|^2)&=0 \\ S_{23}(|S_{12}|^2-|S_{34}|^2)&=0 \end{aligned} \qquad \textbf{(2.3)}$$

To be satisfied the equations (2.3), one way is if if $S_{14}=S_{23}=0$, with results in a directional coupler. Then the self-products of the rows of the unitary S matrix of (2.1) yield the following equation:

$$\begin{aligned} |S_{12}|^2+|S_{13}|^2&=1 \\ |S_{12}|^2+|S_{24}|^2&=1 \\ |S_{13}|^2+|S_{34}|^2&=1 \\ |S_{24}|^2+|S_{34}|^2&=1 \end{aligned} \qquad \textbf{(2.4)}$$

Which implies that $|S_{13}|=|S_{24}|$ and that $|S_{12}|=|S_{34}|$.
There are two commonly used realizations of directional couplers:

The Symmetrical Coupler: the phases of the terms having amplitude β are chosen equal. The S matrix for this device is.

$$[S]=\begin{bmatrix} 0 & \alpha & j\beta & 0 \\ \alpha & 0 & 0 & j\beta \\ j\beta & 0 & 0 & \alpha \\ 0 & j\beta & \alpha & 0 \end{bmatrix} \qquad \textbf{(2.5)}$$

The Antisymmetrical Coupler: the phases of the terms having amplitude β are chosen 180º apart. The S matrix for this device is.

$$[S]=\begin{bmatrix} 0 & \alpha & \beta & 0 \\ \alpha & 0 & 0 & \beta \\ \beta & 0 & 0 & \alpha \\ 0 & \beta & \alpha & 0 \end{bmatrix} \qquad \textbf{(2.6)}$$

It is important to notice that the two couplers differ only in the choice of reference planes and we can see from these matrices S that the network is matched, reciprocal and lossless. Also, the amplitudes α and β are real numbers and are not independent:

$$\alpha^2+\beta^2=1 \qquad \textbf{(2.7)}$$

We can thus conclusion that any reciprocal, lossless, matched four-port network is a directional coupler.

2.1.2 Directional couplers characterization

A figure below illustrates the basic operation of a directional coupler:

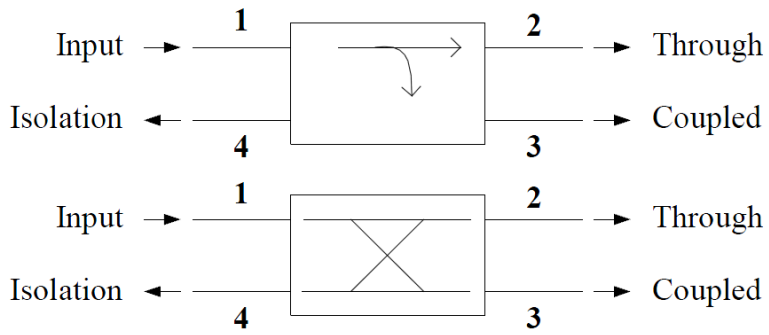

Fig. 2.1 The operations of a directional coupler.

The arrows indicate the assumed directions of time average power flow. We can deduce the operation of this network directly from the S matrix, assuming all the ports are matched. Of course, the directional coupler is not ideal and the S matrix above is only approximately realized in practice, as we can see in annex 4, where S_{11} is not exactly 0.

A directional coupler has four ports, defined as: $P1$ input, where we inject the input signal, $P2$ through which the output signal appears, $P3$ coupled, where we obtain a sample of the input signal and isolated and $P4$, which must be completed by a 50 ohm load (if that were the characteristic impedance of the component) if we want, that works comply with all specifications.

The performance of directional couplers is characterized by the following three values.

2.1.2.1 Coupling C

This parameter gives its name to the component and is considered the most critical in deciding their use and application in an electronic system. The power comes through $P1$, is distributed in a controlled form that leaves between $P2, P3, P4$ and lost along the way, between the doors, $P1-P2, P1-P3$ and $P1-P4$. Coupling is defined as the ratio between the power coming through $P1$ and P3, for a given frequency (we will see that this ratio varies with frequency that we apply to the entry, though we support the constant power for all frequencies). Being a constant value for a defined carrier, if the input power increases $P1$, it is an increase predictive of the power in the coupled port $P3$ and vice versa. We notice that in this way, we can determine the value of the input power, using the information of power in the coupled port, without having to disconnect anything in the circuit.

The expression (2.8) defines the value of the coupling.

$$C(dB)=10\log\frac{P_1}{P_3}=-20\log|S_{13}| \qquad \textbf{(2.8)}$$

Technologically, a directional coupler can be manufactured with the use of appropriate technology, depending on use, the operating frequency, size or power to be borne. However, all technologies are based on the same concept for transferring power from the input to the coupled port. Thus, the value of coupling will vary, depending on the frequency.

To be more precisely, the value of the coupling will vary with the frequency applied to the input port, so that the directional coupler it is useful only in a range of frequencies, which we define as operating frequency.

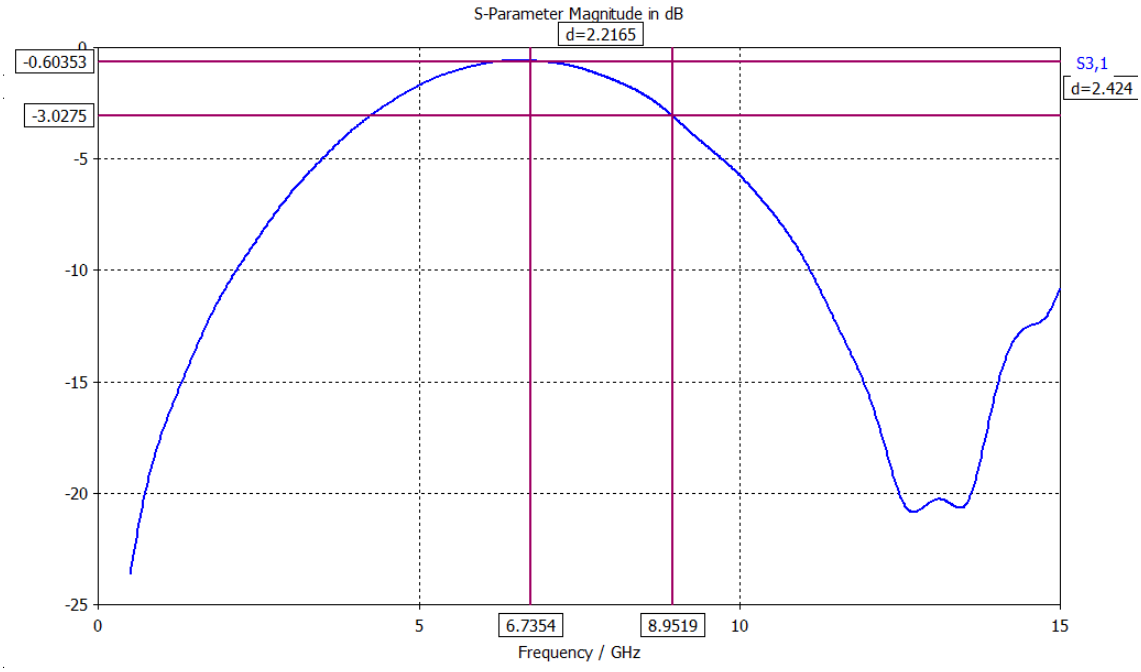

Fig. 2.2 Coupling / Frequency value.

In the Fig. 2.2, we can see what we indicated previously. This is the response of the directional coupler simulated in CST [Annex 4.4.2.1]. A measurement is made between $1-15\,GHz$, with a value of the coupling, which varies with frequency. Thus, $6.7\,GHz$, the coupling is $0.6\,dB$ at $8.9\,GHz$, the coupling value is $3\,dB$ and $12.7\,GHz$, the value of the coupling is $21\,dB$. We can see the response out of 4.5 GHz and above 9Gz, how this decrease sharply.

2.1.2.2 Isolation

It is the power transferred from the through port $P2$, to coupled port $P3$, when the ports $P1$ and $P4$, are terminated by 50 ohm loads.

The expression (2.9) defines the value of the isolation.

$$I\,(dB)=10\log\frac{P_1}{P_4}=-20\log|S_{14}| \qquad \textbf{(2.9)}$$

In the Fig. 2.3, we can see the response of the isolation. This is the response of the directional coupler simulated in CST [Annex 4.4.2.1], the same directional coupler that we used to represent the coupling. It shows once again that the response is not constant and it has values that depend on the frequency. So, for $5GHz$ it has a value of $-25\,dB$, to a value of $-22\,dB$ to 10GHz, and $15GHz$ a value of $-4\,dB$.

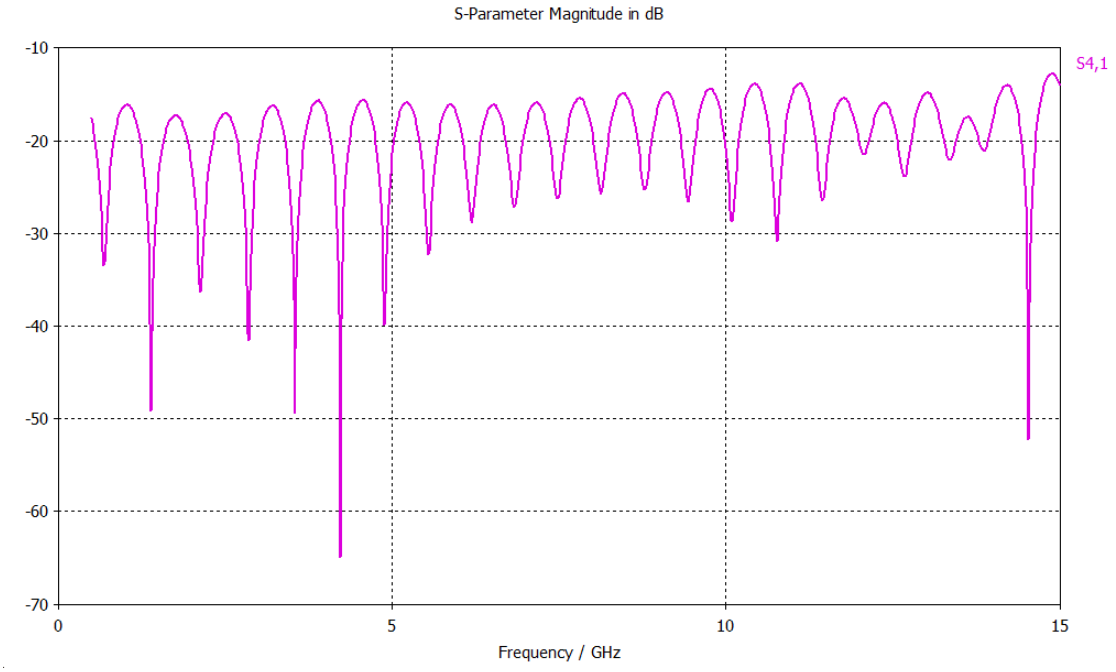

Fig. 2.3 Isolation/Frequency value.

2.1.2.3 Directivity

The directivity is the ability to transfer power from the input port to the coupled port and to reject the power that can come from the through port, due to reflections on this.

From our point of view, it is a parameter that defines the technical and technological quality of directional coupler. The higher value of this parameter is the greater the technical quality of the component will be.

The expression (2.10) defines the value of the isolation.

$$D(dB)=10\log\frac{P_3}{P_4}=-20\log\frac{|S_{31}|}{|S_{14}|} \qquad \textbf{(2.10)}$$

We can also define the directivity as a measure of the coupler's ability to isolate forward and backward wave, as is the isolation. These quantities ca be related as:

$$I=D+C\,dB \qquad \textbf{(2.11)}$$

In the Fig. 2.4, we can see the response of the directivity, using the equation (2.11) in MatLab. This is the response of the directional coupler simulated in CST [Annex 4.x], the same directional coupler that we used previously. It shows once again that the response is not constant and it has values that depend on the frequency. So, in the frequency band of $4-10\,GHz$ we have $10-15\,dB$ of directivity.

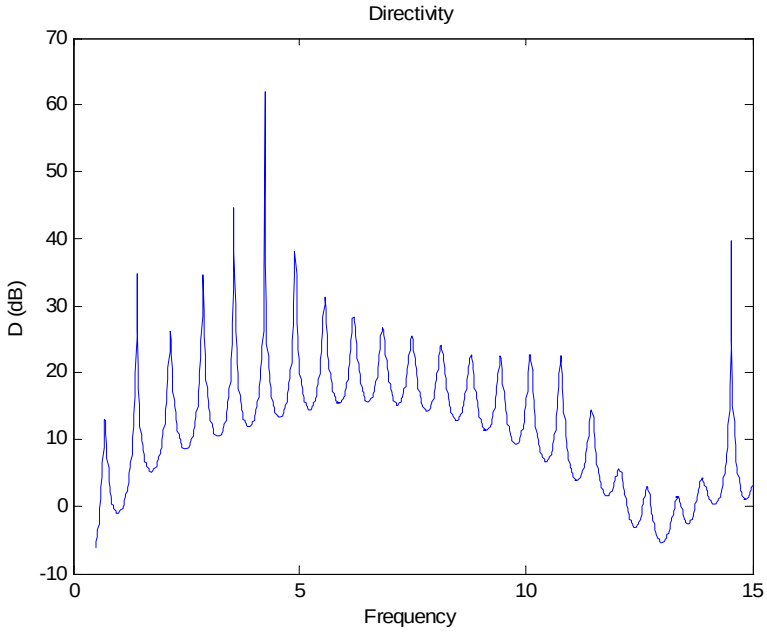

Fig. 2.4 Directivity/Frequency value.

A reduced value of directivity has a bad influence, not only limiting the accuracy of a reflectometer, but also with the capacity of producing deviations in the coupled power level from a coupler. These phenomena appear even in the case of a minor discrepancy on the through line.

In general terms, we cannot make a direct measurement of the directivity of a coupler due to the fact that it involves a low-level signal, which has the possibility of being camouflaged by the coupled power from a reflected wave on the through arm.

The left-hand figure further down, illustrates one possible way to quantify coupler directivity using a sliding matched load. It initiates with the coupler connection to a source and matched load and the measurement of the coupled output power. Taking into consideration an input power P_i, will result an output power $P_c = C^2 P_i$. In the context, $C = 10^{(-CdB)/20}$ is the numerical voltage coupling factor of the coupler. Further steps we will be to reverse the position of the coupler as presented in the right-hand figure and terminate the through line with a sliding load.

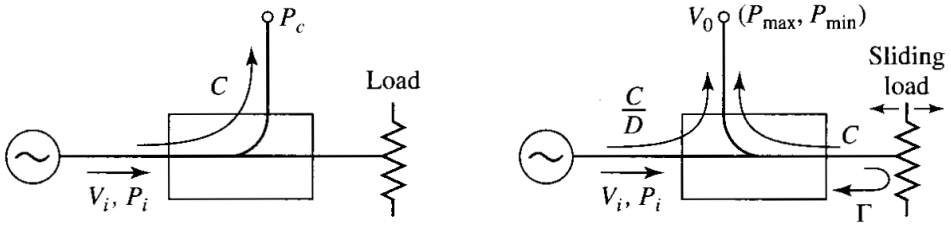

Fig. 2.5 Practical measurement of directivity.

It is important to mention that the changing of the position of the sliding load brings in a variable phase shift in the signal that is reflected from the load and coupled to the output port. This phase is the path length difference between the directivity and reflected signals. Then the minimum and maximum output powers are by:

$$P_{min} = P_i \left(\frac{C}{D} - C|\Gamma| \right)^2 \quad , \quad P_{max} = P_i \left(\frac{C}{D} + C|\Gamma| \right)^2 \qquad \textbf{(2.12)}$$

M and m will be taken into consideration in the following way:

$$M = \frac{P_c}{P_{max}} = \left(\frac{D}{1 + |\Gamma| D} \right)^2 \quad , \quad m = \frac{P_{max}}{P_{min}} = \left(\frac{1 + |\Gamma| D}{1 - |\Gamma| D} \right)^2 \qquad \textbf{(2.13)}$$

These ratios can be accurately measured directly by using a variable attenuator between the source and coupler. The directivity (numerical) can then be found as:

$$D = M\left(\frac{2\mathrm{m}}{m+1}\right) \qquad \textbf{(2.13)}$$

This method (look [2]) requires that $|\Gamma| < 1/D$ or, in dB, $RL > D$.

2.1.2.4 Loses

When we are speaking about looses, we fundamentally must consider two types of loses: those of insertion, that are taking place in the road from $P1$ to $P2$, and those of coupling, that are taking place in the road from $P1$ to $P3$. We do not take into consideration those produced because of the reflection and those dissipative because they are less significant comparing with the first mentioned ones.

2.1.2.4.1 Loses of insertion

This kind of loses take place in the main road between the entrance and the exit of the directional coupler $P1-P2$ and are related with the transmission environment that join the two ports.

2.1.2.4.2 Loses of coupling (dB)

This kind of loses are produced in the power coupling form the main road at coupler $P1-P3$. Its value is related to the quantity of power coupled, to be more precisely, the more signal is transferred at the coupler port, higher will be the lose and vice versa.

In the Table 1 we can observe some values of coupling with their correspondent loses of insertion and loses of coupling. In the right handed it is indicated in % the ratio of loses of coupling in the total amount of coupler loses. We can observe that starting with couplings higher than 20 dB, the loses of coupling are reduced, 9% of total loses. But for reduced values of coupling (coupling of 6 dB), the loses of coupling represent 75% of the loses, drastically affected by the present power at the exit port $P2$.

Coupling (dB)	Insertion (dB)	P.Coupler	P.Totals	% P.Coupler
6	0.4	1.2	1.6	75
11	0.4	0.46	0.86	53
15	0.4	0.14	0.54	25
20	0.4	0.04	0.44	9
30	0.4	0.004	0.0404	0.99

Table 2.1 Contribution of losses.

2.1.3 Coupled line theory

Coupled transmission lines appear as a consequence of two unshielded transmission lines that are close together, due to the fact that power can be coupled between the lines thanks to the interaction of the electromagnetic fields of each line. Even if mostly of coupled transmission lines consist of three conductors close together, there is the possibility of more conductors being used. In the Fig. 2.6 we get a clear image of different coupled transmission lines, but in our study, we focus on the study of microstrip.

Most of the times coupled transmission lines are operating in the TEM mode, mode studied in the first chapter, which is absolutely valid for stripline structures, but only partial valid for microstrip structures. Technically a three-wire line, as those presented in Fig. 2.6, are able to support two distinct propagating modes, a very important characteristic that can be exploited to implement directional couplers, hybrids, and filters.

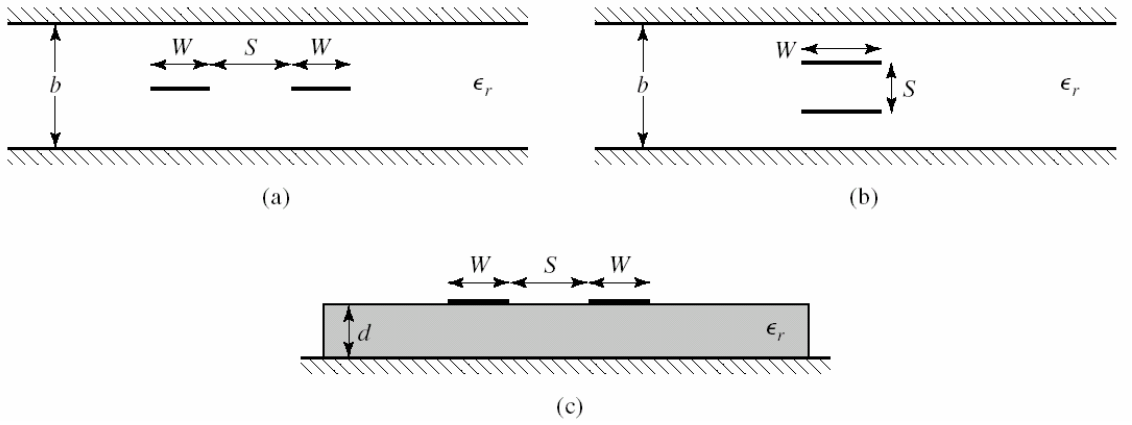

Fig. 2.6 Various coupled transmission line geometries. (a) Coupled stripline: planar or edge-coupled, (b) Coupled stripline: stacked or broadside-coupled, (c) Coupled microstrip.

Taking a look at the Fig. 2.7, C_{12} correspond to the two strip conductors in the lack of the ground conductors, as the same time as C_{11} and C_{22} illustrate the capacitance between one strip conductor and the ground conductor in the lack of the second strip conductor. Supposing that the two strips are equal in dimension and location, in relation to the ground one we can further say that $C_{11} = C_{22}$. We are considering the ground conductor to be the third one for this conductor's often assumed role in many applications as the ground plane of a stripline or a microstrip circuit.

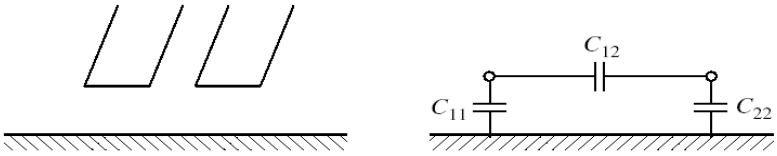

Fig. 2.7 A three-wire coupled transmission line and its equivalent capacitance network.

The Fig. 2.8 offers a clear image for the electric field lines in the cases of two special types of excitations for the coupled line. First we analyze the situation of the even mode, when the currents in the strip conductors are identical regarding the amplitude and the direction, and second the odd mode which is dealing with identical amplitude conductors with opposite directions.

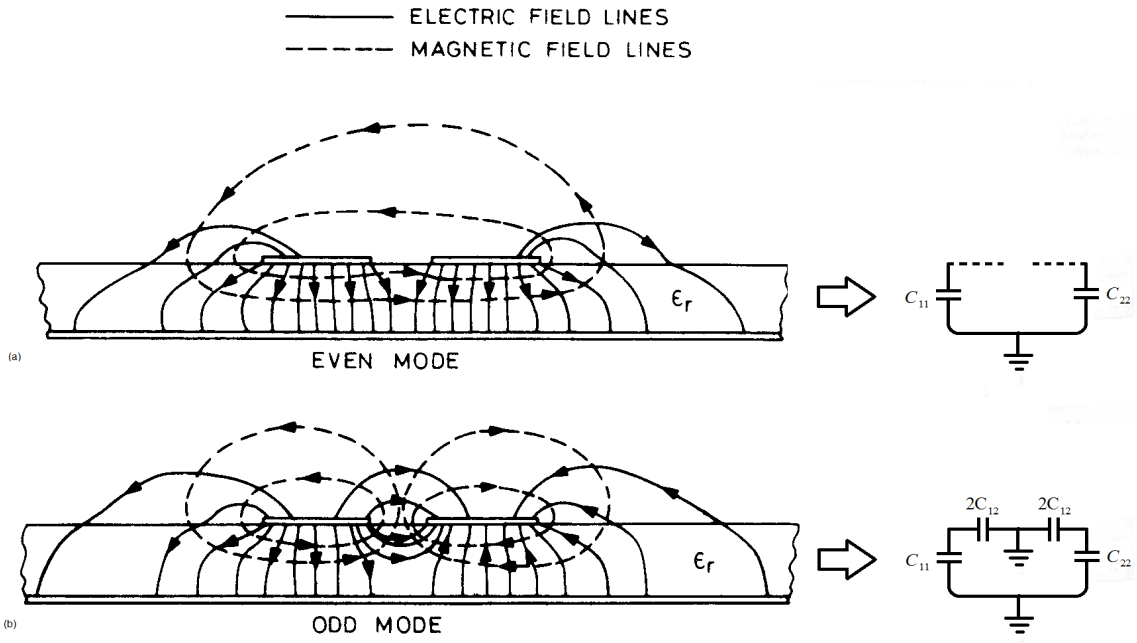

Fig. 2.8 Even and odd mode excitations for a coupled line and the resulting equivalent capacitance networks.
(a) Even-mode excitation
(b) Odd-mode excitation

For the even mode, the electrical field has even symmetry about the center line, and no current flows between the two strip conductors. We have the following resulting capacitance of either line to ground $C_e = C_{11} = C_{22}$ and the following characteristic impedance:

$$Z_{0e} = \sqrt{\frac{L}{C_e}} = \frac{\sqrt{LC_e}}{C_e} = \frac{1}{vC_e} \qquad \textbf{(2.14)}$$

where v represents the velocity of propagation on the line.

In the Fig. 2.9, we can see the graphic representation of the even mode. This is the representation of the directional coupler simulated in CST [Annex 4.4.2.1], This simulation is also used for the odd mode. The figure on the left is the absolute value of the magnetic field and the right figure is the absolute value of the electric field, both represented at the same point of the coupled. We are going to see in the next chapter how we have performed these simulations.

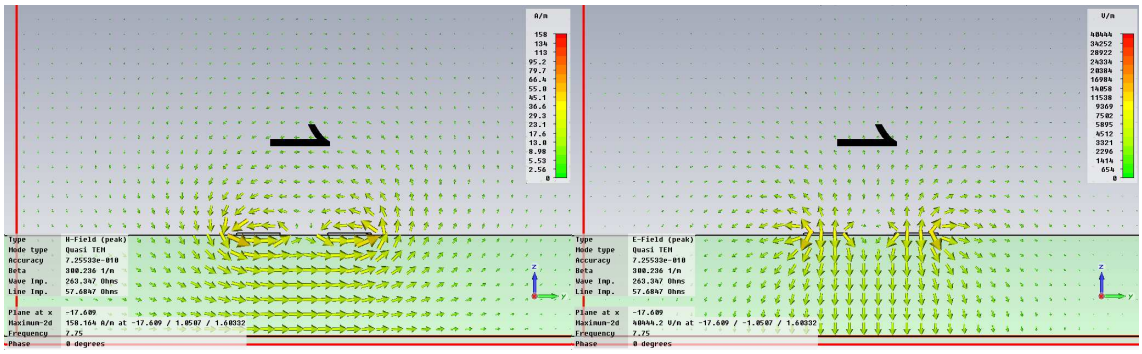

Fig. 2.9 Simulation of even mode excitations for a coupled line.

Talking about the odd mode, we can notice a voltage null between the two strip conductors and an odd symmetry about the center line. We can express the effective capacitance between a strip conductor and the ground one as it follows, $C_0 = C_{11} + 2C_{12} = C_{22} + 2C_{12}$. In this case the characteristic impedance takes the form below:

$$Z_{0o} = \frac{1}{vC_o} \qquad \textbf{(2.15)}$$

Z_{0e} and Z_{0o} represent the characteristic impedances of one strip conductor in relation to the ground conductor in the two situations of the coupled line operation.

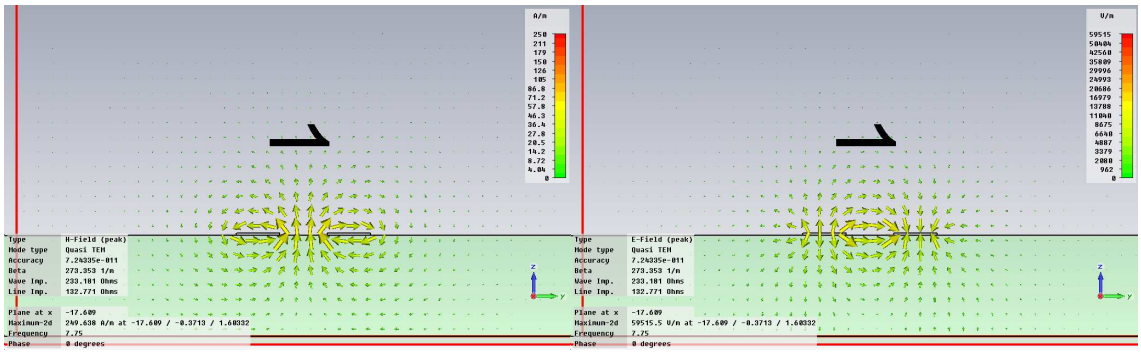

Fig. 2.10 Simulation of odd mode excitations for a coupled line.

In the Fig. 2.10, we can see the representation of the odd mode. This is the representation of the directional coupler simulated in CST [Annex 4.4.2.1], the figure on the left is the absolute value of the magnetic field and the right figure is the absolute value of the electric field, both represented at the same point of the coupler.

We are going to see in the next chapter how we have performed these simulations.

In the situation of a purely TEM coupled line, like coaxial, parallel plate or stripline, it is possible to evaluate the capacitances per unit length of line using conformal mapping, and then determine the characteristic impendances. In the situation of quasi-TEM lines, like microstrip, there is the possibility to arrive at these results numerically or by approximate quasi-static techniques.

An important thing to mention is that for microstrip the design graphs must be made for specific values of dielectric constant, because the results to not scale with dielectric constant.

Another problem regarding the microstrip coupled lines is that the phase velocity is normally different for the two model of propagation, thing that has a degrading influence on the directivity of the coupled lines.

The following figure presents a example of graphical design data for microstrips with $\epsilon_r = 10$.

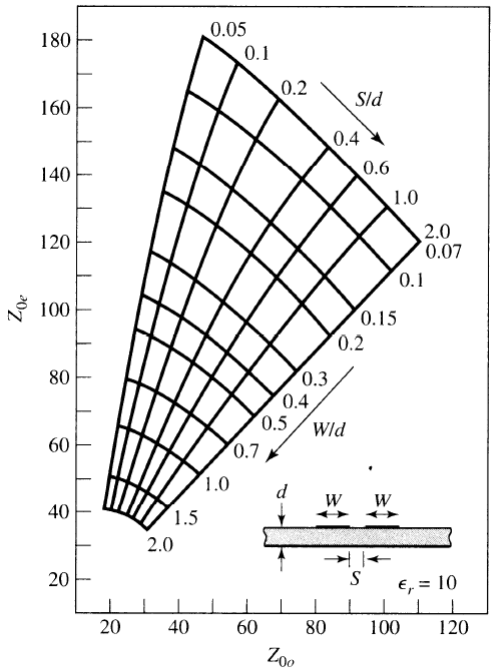

Fig. 2.11 Even and odd mode characteristic impedance design data for coupled microstrip lines.

With the preceding definitions of the even and odd mode characteristic impedance, we can apply an even-odd mode analysis to a length of coupled line to arrive at the design equations for a single-section coupled line coupler. Such a line is shown in Fig. 2.12.

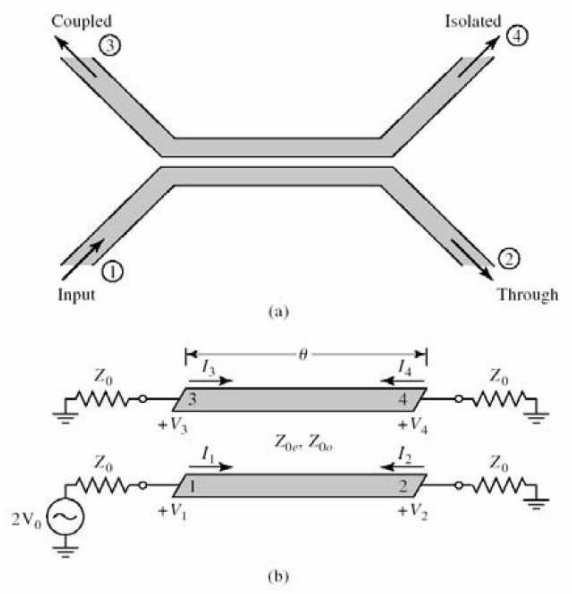

Fig. 2.12 A single section coupled line coupler. (a) Geometry and port designations. (b) The schematic circuit.

The coupled line directional coupler is excited at port 1 and terminated with Z_0 at all ports.

For this problem we will apply the even-odd mode analysis technique in conjunction with the input impedances of the line, as opposed to the reflection and transmission coefficients of the line. So by superposition, the excitation at port 1 in Fig. 2.12 can be treated as the sum of the even and odd mode excitations shown in Fig. 2.13.

By symmetry, we can deduce that for this even mode problem:

$$I_3^e = I_1^e \quad , \quad I_4^e = I_2^e$$
$$V_3^e = V_1^e \quad , \quad V_4^e = V_2^e \qquad \textbf{(2.16)}$$

while for the odd:

$$I_3^o = -I_1^o \quad , \quad I_4^o = -I_2^o$$
$$V_3^o = -V_1^o \quad , \quad V_4^o = -V_2^o \qquad \textbf{(2.17)}$$

By definition:

$$Z_{in} = \frac{V_1}{I_1} = \frac{V_1^e + V_1^o}{I_1^e + I_1^o} \qquad \textbf{(2.18)}$$

These transmission line problems in Fig. 2.12 are simple and easy to solve. As shown in the text, by choosing:

$$Z_0 = \sqrt{Z_{0e} Z_{0o}} \qquad \textbf{(2.19)}$$

leads to:

$$Z_{in} = Z_0 \qquad \textbf{(2.20)}$$

That is, with (2.19) then port 1 is matched and given the symmetry of structure, all ports will then be matched.

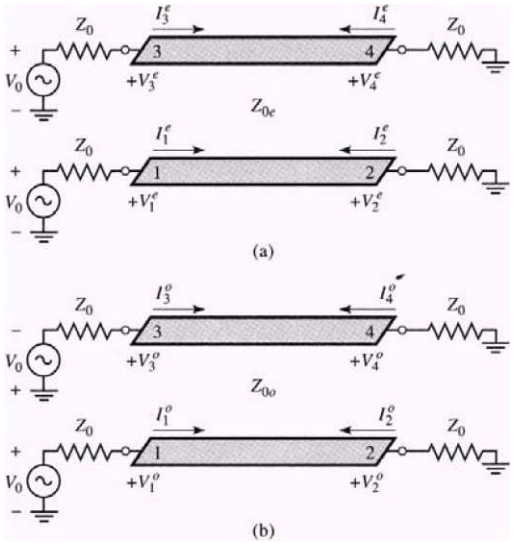

Fig. 2.13 Decomposition of the coupled line coupler circuit of Fig. 2.12 into even and odd mode excitations. (a) Even mode. (b) Odd mode.

Now if (2.19) is satisfied, we have that:

$$V_1 = V$$

$$V_2 = V\frac{\sqrt{1-C^2}}{\sqrt{1-C^2}\cos\theta + j\sin\theta} \qquad \textbf{(2.21)}$$

$$V_3 = V\frac{jC\tan\theta}{\sqrt{1-C^2}\,j\sin\theta}$$

$$V_4 = 0 \quad (total\ isolation)$$

where $\theta = \beta l$ is the electrical length and is the voltage coupling coefficient. (Here, C stands for " coupling", not "capacitance").

$$C = \frac{Z_{0e} - Z_{0o}}{Z_{0e} - Z_{0o}} \qquad \textbf{(2.22)}$$

The second and third equations of (2.21) can be used to plot the coupled and through port voltage versus frequency, as chow in Fig.2.14. At very low frequencies ($\theta \ll \pi/2$), virtually all power is transmitted through port 2, with none being coupled to port 3. For $\theta = \pi/2$ the coupling to port 3 is at its first maximum; this is where the coupler is generally operated, for small size and minimum line loss. Otherwise, the response is periodic, with maximum in V_3 for $\theta = \pi/2, 3\pi/2, \ldots$.

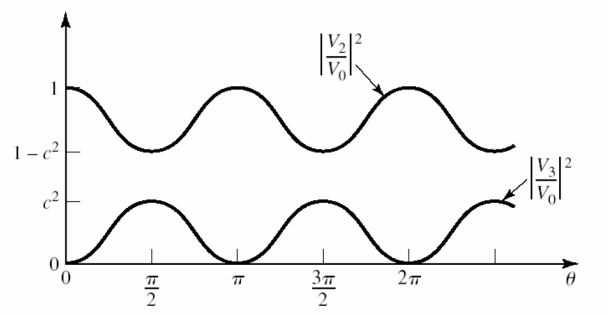

Fig. 2.14 Coupled and through port voltage (squared) versus frequency for the coupled line coupler of Fig. 2.12.

For $\theta=\pi/2$ the coupler is $\lambda/4$ long, and (2.21) reduce to:

$$\frac{V_3}{V}=C$$
$$\frac{V_2}{V}=-j\sqrt{1-C^2} \qquad \textbf{(2.23)}$$

which shows that $C<1$ is the voltage coupling factor at the design frequency, $\theta=\pi/2$. Note that these results satisfy power conservation. Also observe that there is a 90º phase shift between the two output port voltages; thus coupler can be used as a quadrature hybrid. And, as a long as (2.19) is satisfied, the coupler will be matched at the input and have perfect isolation, at any frequency.

Finally, if the characteristic impedance, Z_0, and the voltage coupling coefficient, C, are specified, then the following design equations for the required even and odd mode characteristic impedances can be easily derived from (2.19) and (2.22):

$$Z_{0e}=Z_0\sqrt{\frac{1+C}{1-C}}$$
$$Z_{0o}=Z_0\sqrt{\frac{1-C}{1+C}} \qquad \textbf{(2.24)}$$

In the above analysis, we assumed that the even and odd modes of the coupled line structure have equal velocities of propagation, so that the line has the same electrical length for both modes. For a coupled microstrip, or other non-TEM, line this condition will generally not be satisfied, and the coupler will have poor directivity. An explanation for the fact that coupled microstrip lines have unequal

even and odd mode phase velocities can be realised by considering the field line plots of Fig. 2.8, which show that the even mode has less fringing field in the air region than the odd mode. This is why its effective dielectric constant should be higher, indicating a smaller phase velocity for even mode.

The use of dielectric overlays and anistropic substrates is included in the techniques for compensating coupled microstrip lines in order to achieve equal even and odd mode phase velocities

We can state that this type of coupler is best suited for weak couplings, as tight coupling requires lines that are too close together to be practical, or a combination of even and odd mode characteristic impedance that would be nonrealizable.

CHAPTER 3 SIMULATION IN CST

3.1 What is CST STUDIO SUITE™?

The electromagnetic simulation software CST STUDIO SUITE™ is the culmination of many years of research and development into the most efficient and accurate computational solutions to electromagnetic design. It comprises CST's tools for the design and optimization of devices operating in a wide range of frequencies, static to optical. Analyses may include thermal and mechanical effects, as well as circuit simulation. All programs are accessible through a common interface with facilitates circuit and multi-physics co-simulation.

CST STUDIO SUITE comprises different modules for different applications. In the following simulations use the CST MWS module to study directional couplers of coupled microstrip lines.

CST MICROWAVE STUDIO® (CST MWS) is a specialist tool for the fast and accurate 3D EM simulation of high frequency problems.

3.2 A microstrip

To introduce the topic of simulations of microstrip lines with CST, we carry out a simple example, simulating a single microstrip line.

To obtain physical parameters of the microstrip line can use a tool called TX-Line (Transmission Line Calculator). TX-Line is a free, easy-to-use, interactive transmission line calculator for the analysis and synthesis of transmission line structures. TX-Line enables users enter either physical characteristics or electrical characteristic for common transmission medium.

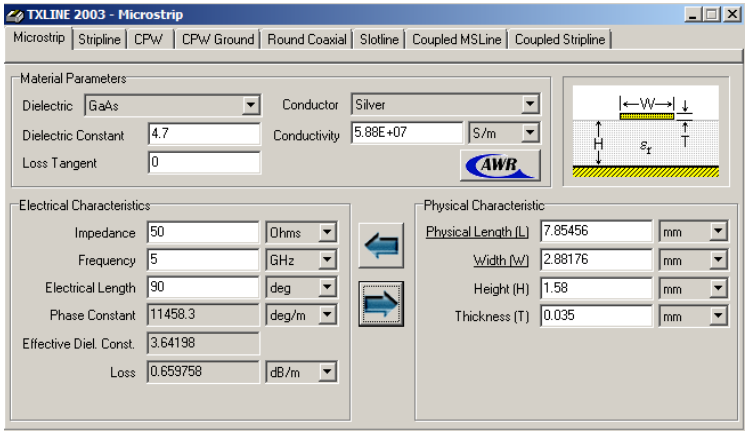

Fig. 3.1 TX-Line (Transmission Line Calculator).

Entering material parameters and the electrical characteristics used, this program gives us the physical characteristics, or vice versa. In the above figure we can see the program window and data used for the simulation of a microstrip line.

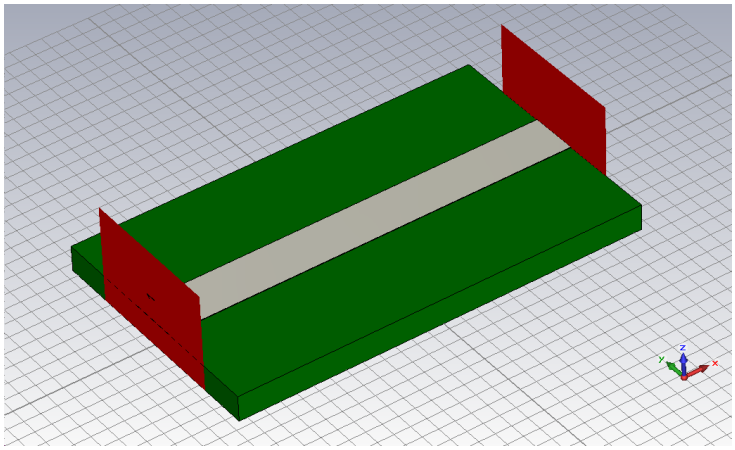

Fig. 3.2 A microstrip line in CST.

With the CTS program design the structure of the line in three dimensional spaces. For all simulation using the default conductor and the dielectric material is copper, which has the effective dielectric constant $\epsilon_r = 4{,}7$.

The red regions we can see in Fig 3.2 represent ports of input and output. This allows us to obtain graphics such as the coefficient of S matrix, the Smith chart, electrical field, magnetic field, etc. In [Annex 4.4.1] we can find the graphs of the coefficients of the S matrix for the simulation of a microstrip line.

3.3 Two coupled lines

As we have seen in the previous chapter, we have introduced graphics to discuss the characteristics of a directional coupler. These graphs are extracted from the following example simulated with CST (Fig. 3.4).

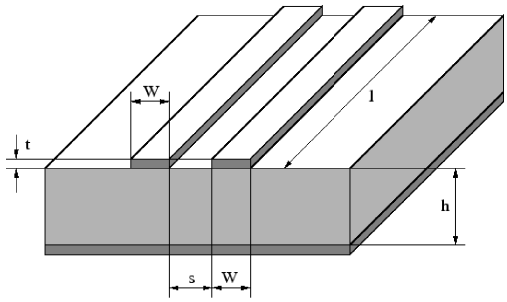

Fig. 3.3 Coupled microstrip lines.

To make the study of this directional coupler, we decided to set three parameters (Fig 3.3). We can used as realistic values, the same used in the simulation of a microstrip line: $h=1.58\,mm$, $t=0.035\,mm$ and copper dielectric constant $\epsilon_r=4{,}7$.

The possible values of S and W, which is available in coupled microstrip lines are as follows (look [5]):

$$0{,}1\leqslant W/h\leqslant 10 \quad , \quad 0{,}1\leqslant S/h\leqslant 5 \qquad \textbf{(3.1)}$$

The following figure is three-dimensional representation of two microstrip transmission lines coupled with $W=1.5\,h$ and $S=0.7\,h$.

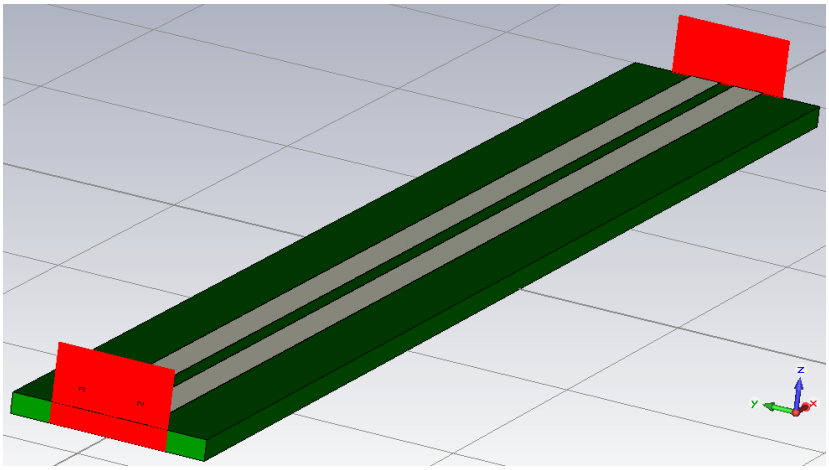

Fig. 3.4 Coupled microstrip lines in CST.

To understand the operation of the designed directional coupler (Fig. 3.4), first we must observe the coefficient of S matrix S_{31} , [Annex 4.4.2.1]. This graph has been discussed in the previous chapter, to explain the coupling. The frequency, which have the largest coupling is $f=6.73\,GHz$. The operating band of the directional coupler depend on how strict we are with the coupling, if we can tolerate a $3\,dB$ of coupling, we will be a operation band about $4.4\,GHz$.

To know what happens in the difference outputs of the directional coupler, we can look the other coefficients of the S matrix. For example, S_{11} [Annex 4.4.2.1], has small values. Another important factor is the insertion loss. Losses that occur on the main road between input and output directional coupler $P1-P2$ and these are related to the transmission medium that connects the two ports S_{21} . We can see in the figure below that these are taking minimum values in the frequency $f=6.73\,GHz$, but increase as we move of frequency.

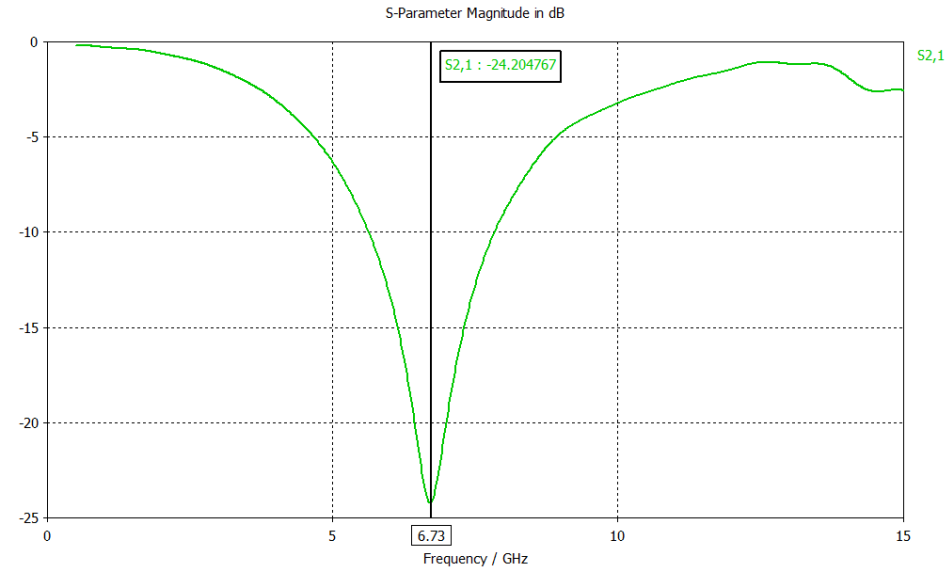

Fig. 3.5 The insertion loss of the coupled microstrip lines.

The CST MWS program allows you to simulate the magnetic fields and electric fields along the transmission line. Thus we have an idea of coupling between the lines and the behavior of the fields through the lines. The program also allows us to make an animation of the magnetic fields and electric in the transmission lines.

The following figure shows a picture of the animation of magnetic field at frequency $f = 6.73\,GHz$, where we can see perfectly the transmission power of a microstrip line to the other.

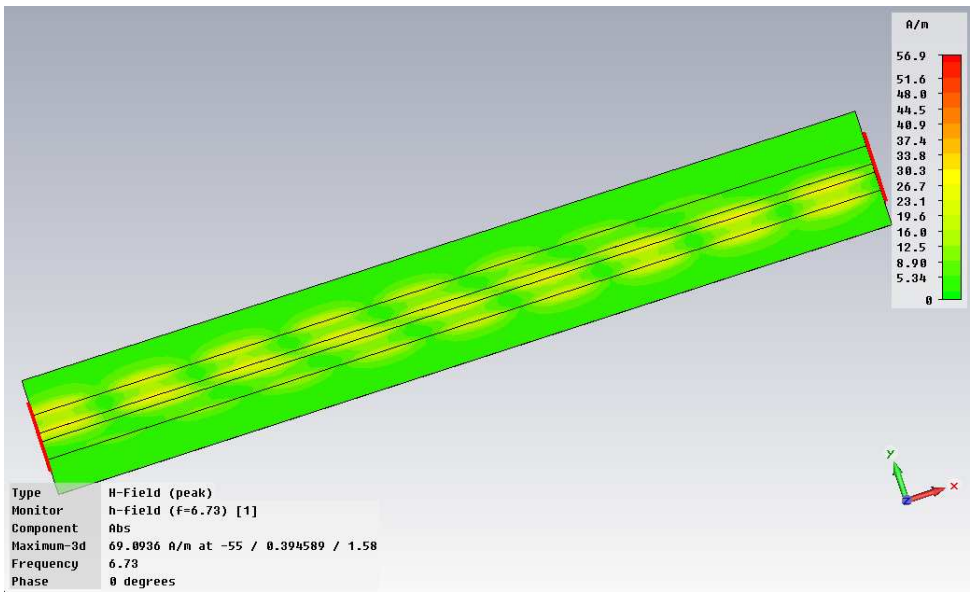

Fig. 3.6 Magnetic field of the coupled microstrip lines.

We have realized all the simulations with the same signal of entrance. The CST MWS have a default excitation signal. Like we can observe in the following graphic, that signal represents the unitary Gaussian function.

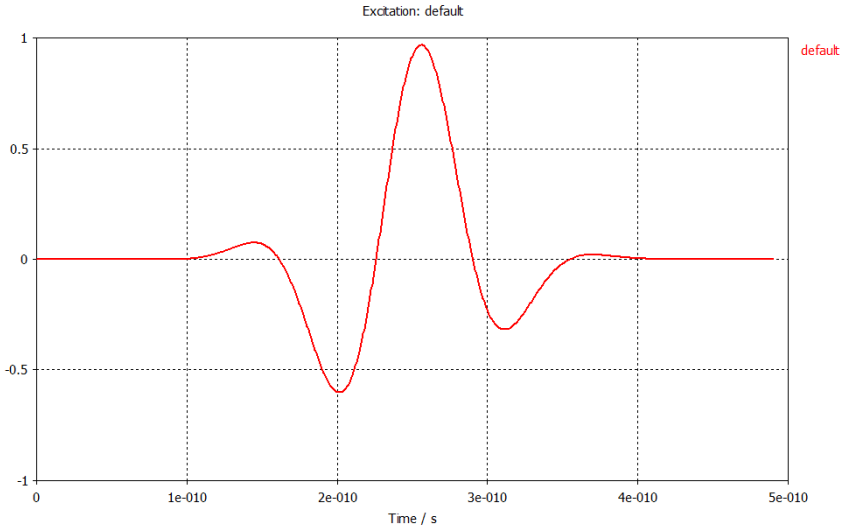

Fig. 3.7 Default excitation signal.

The CST MWS allows us to study the comportament of the magnetic field and of the electric field in a point of line in time. The following graphic we can observe the electric field in a point l .

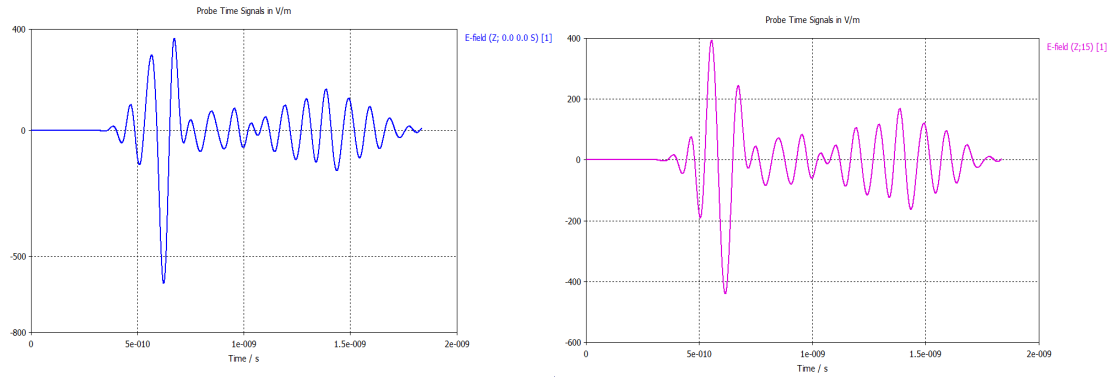

Fig. 3.8 Electrical field of the coupled microstrip lines in a point l (2 lines).

We can see how the signal delays above $3 \cdot 10^{10}\, s$ for this distance l and at this instance our signal is not exactly like the original one. We can also state that l is a point for the center of the line because there is about the same signal of electric field in the two lines. We can observe at the final of the line that the line 2 would practically have the full power.

Annex 4 we can find all the figures of the simulation results.

Now varying physical parameters of the directional coupler, we add the effects caused. These are the most interesting cases we have seen in the CST MWS simulation of several examples.

3.3.1 Length of the line (parameter l)

The following figure shows the simulation of the directional coupler but with only one variation, the transmission line length is doubled.

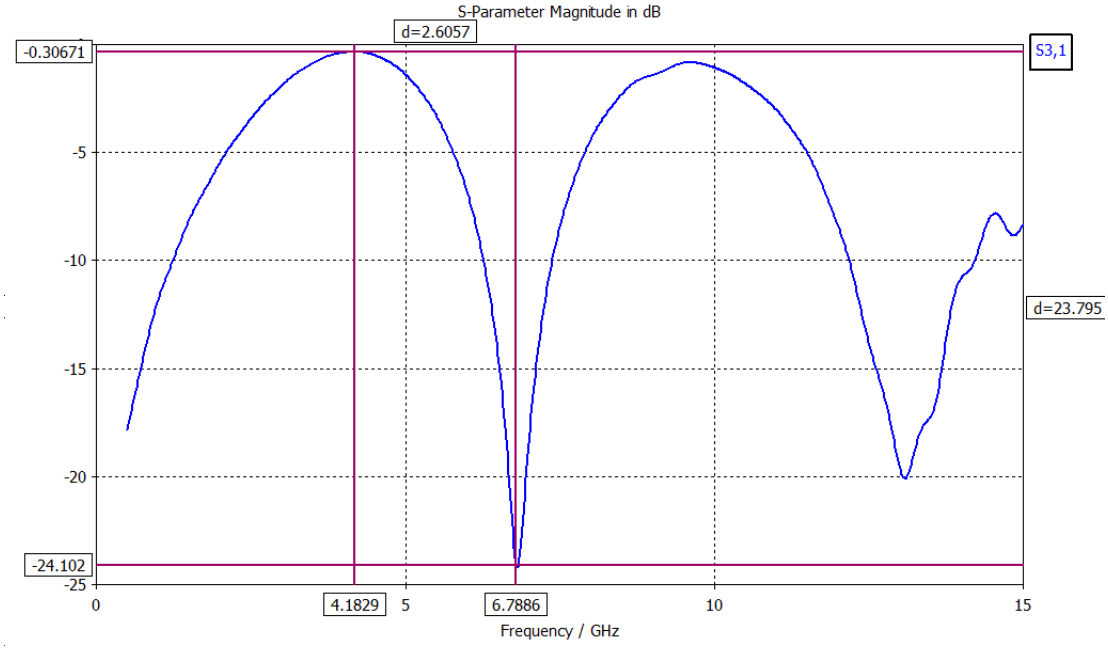

Fig. 3.9 Coupling / Frequency value.

We can see in Fig. 3.9 that the frequency of work $f = 6.73\,GHz$, we have the second minimum of the function by doubling the length of the lines.

With this effect we have managed to increase by two the frequency of the function and S_{21} and S_{31} [Annex 4.4.2.2], of the new directional coupler. The responses of these functions are always periodic.

To know the effects we have doubled the frequency in the magnetic field and electric field in the transmission lines to the same operating frequency $f = 6.73\,GHz$, fact represented in the following figure.

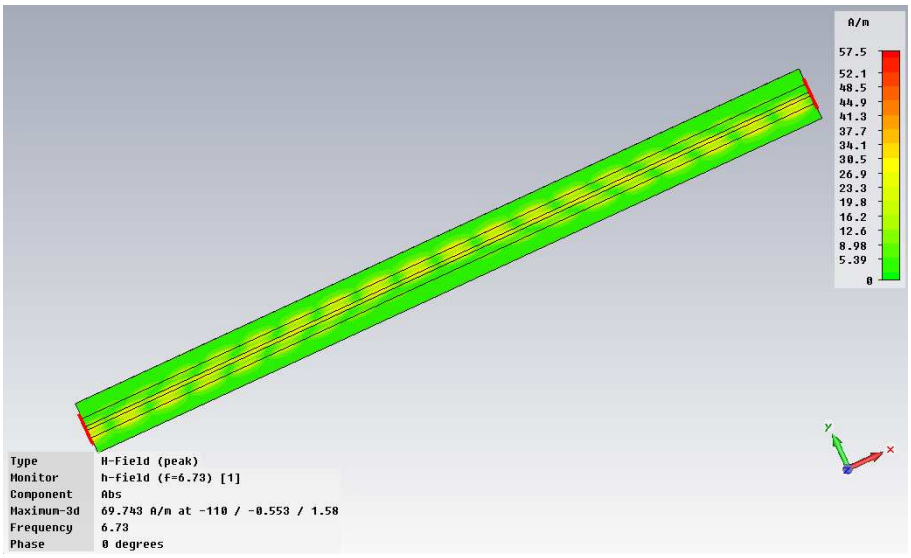

Fig. 3.10 Magnetic field of a coupled microstrip lines.

In the Fig 3.10 we see how, up to the half of the line, the magnetic field is transferred of the same form that the other directional coupler (Fig. 3.6). With this experiment we can say that this directional coupler behaves like two of the half length to gather (Fig. 3.6).

3.3.2 Separation between lines (parameter S)

To determine the effect of varying the distance between the coupled lines, we present the most significant example, where we increase the separation between lines to $S = h \cdot 4$, to see the results.

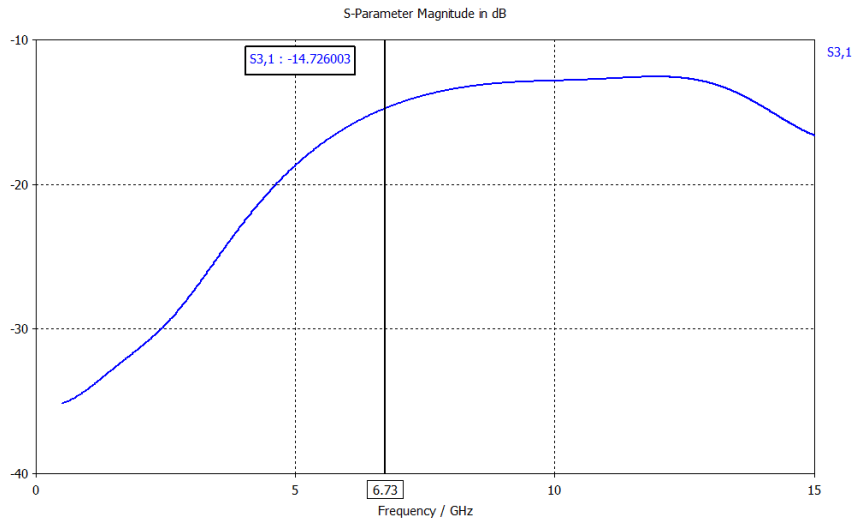

Fig. 3.11 Coupling / Frequency value.

The most significant effect of increasing S, we can see it clearly in the graph above S_{31}, is a reduction of about $13\,dB$ coupling. All other graphics of this simulation are in [Annex 4.4.2.3].

With this experiment we can say that we design the directional coupler to the distance between coupled lines relatively small in terms all other parameters as the input signal, the height of the dielectric, etc ... . In order not to worsen the coupling.

3.3.3 Width of transmission lines (parameter W)

We have performed several simulations varying the width of the lines and we realized that the most important effect is a change in the operation of our band directional coupler.

The following figure is represented the coefficient of the matrix S_{31} in dB of example, in which we increase the width of the two equal lines $W = 4 \cdot h$.

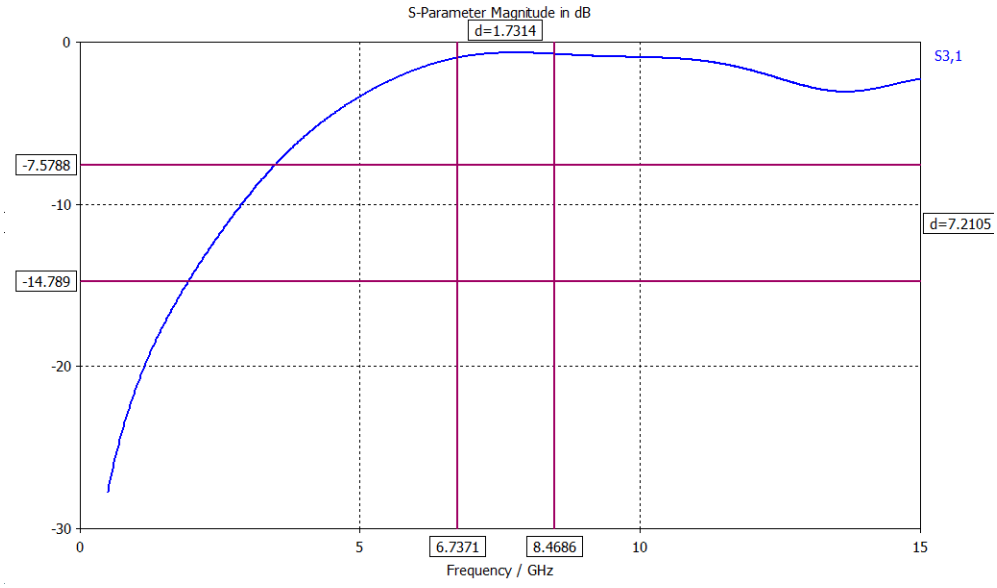

Fig. 3.12 Coupling / Frequency value.

In this example we can see that we have a coupling of $1\,dB$, a wide band of frequencies, from $6.7\,GHz$ to about $12\,GHz$.

3.4 Three coupled lines

We have studied the coupled lines of three lines and now we want to study the comportment adding one more line. In this section we realize similar simulations.

In this design we had to add two ports for the new transmission line.The following figure is three-dimensional representation of three microstrip transmission lines coupled with $W=1.5h$ and $S=0.7h$.

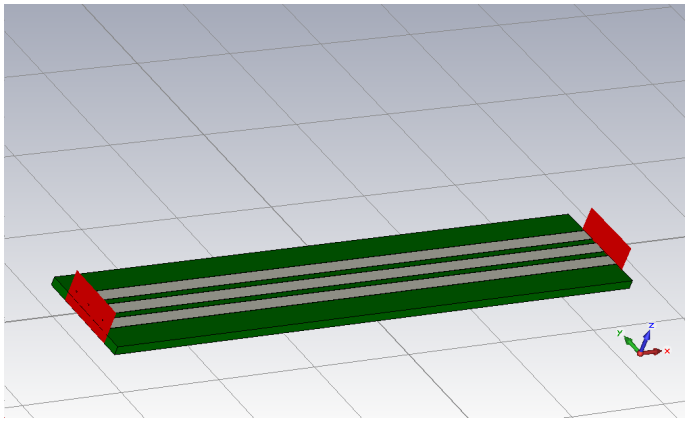

Fig. 3.13 Three coupled microstrip transmission lines.

The following figure represents the coupling for a two-line directional coupler if it was not the third line. The (Fig 3.4),that have been seen previously has been designed with the same parameters but only with two lines. If we are looking the coupling of the directional coupler [Annex 4.4.2.1], we can see how is changing the function form, changing the minimum from -20dB , from $13.5GHz$ to 9GHz , allowing to design a coupler on 9GHz .

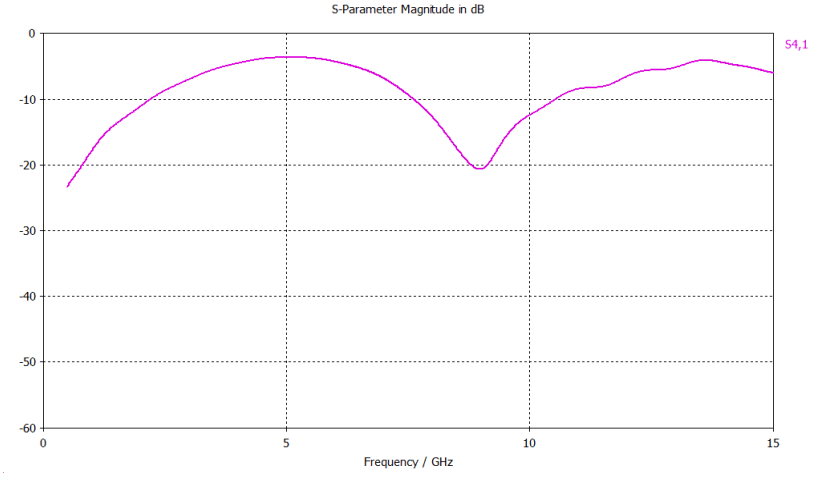

Fig. 3.14 S_{41} parameter.

Like we can see in [Annex 4.4.3.1] the parameter S_{21} shows us that the design has less looses of insertion in the frequency $9.8\,GHz$.

We can define the S_{61} parameter to be the coupling of the coupler of three lines.

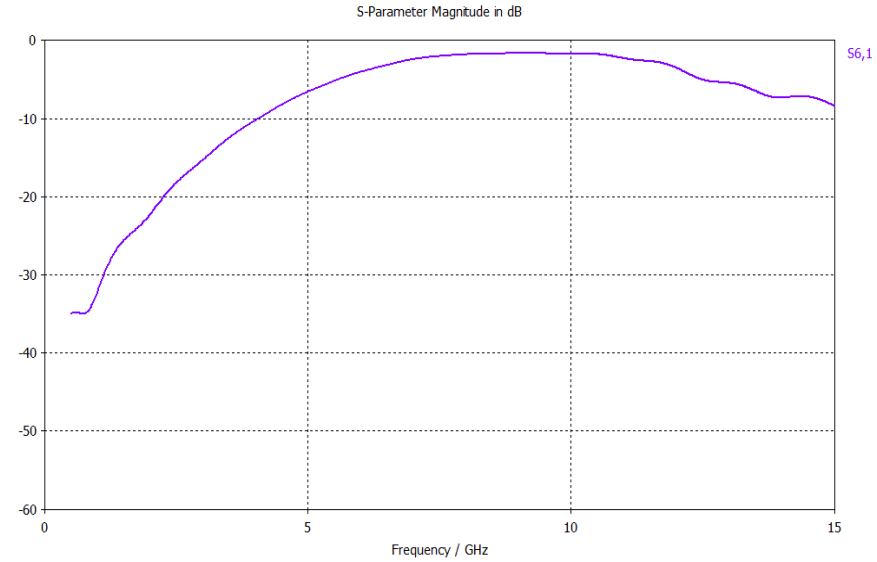

Fig. 3.15 Coupling / Frequency value.

Comparing always with the coupling of two lines, we can see how the design has a major band we can see how the design has a higher operating band.

These three coupled microstrip transmission lines have a major coupling at the frequency of operating of $9\mathrm{GHz}$. In the following figure we can observe how in this frequency, there is transmission of power from the first line to the third.

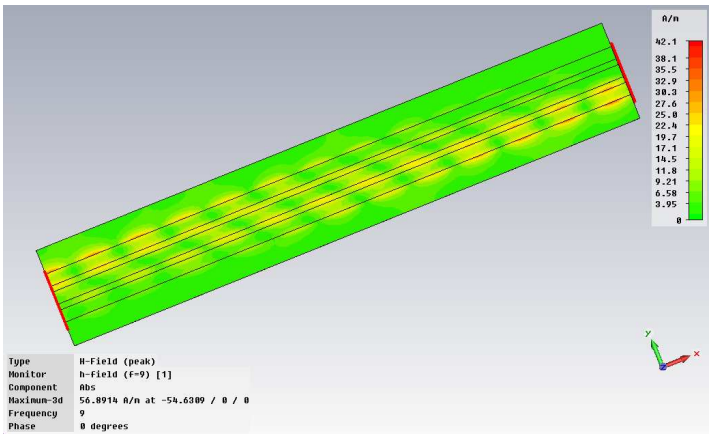

Fig. 3.16 Magnetic field of the coupled microstrip lines $(f = 9\mathrm{GHz})$

For studing this coupler of three lines coupling we have realized similar simulations like those for studing the two lines coupler. Some tests have the same effects, like for example the variation of the length parameter. The most significant simulations there are in [Annex 4.4.3]. Following we present some of them.

3.4.1 Separation between lines (parameter S)

One of the tests has been increased the distance between the lines , so we realized that increasing the distance is loosing more coupling that coupling of two lines.

The following graphic shows a simulation of the same design previously presented (Fig. 3.13) but changing the parameter $S=4\mathrm{h}$.

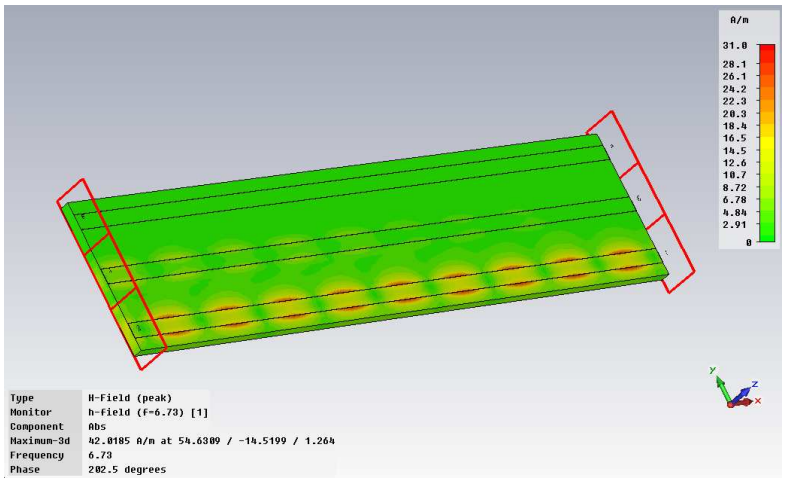

Fig. 3.17 Magnetic field of the coupled microstrip lines $(f=6.73\mathrm{GHz})$

We observe that the signal is not coupling at the third line, remaning at the maximum power in the port 2 of the first line. We have realized the simulation of the magnetic field of this frequency, because like we can see in the graphic the parameter S_{61} [Annex 4.4.3.2] we have a maximum at the frequency $6.73\,GHz$ of $20\mathrm{dB}$ of coupling.

3.4.2 Width of transmission lines (parameter W)

We realize the same experiment with that of coupler of two lines. We make a variation in the value of the line of transmission width for seeing the effects in the exit of the ports. We are waiting for similar effects.
The following graphic shows the parameter S_{21} of coupler of three lines microstrip with $W=3\,h$ and $S=0.7\,h$.

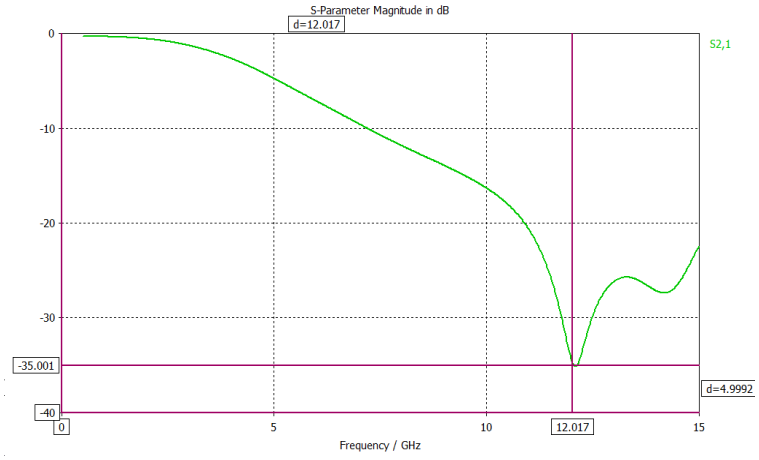

Fig. 3.18 S_{21} parameter.

It is confirmed that increasing the width of line, the three microstrip transmission lines works better for a higher frequency. We can also see that there are less looses of insertion because we have -35dB of S_{21} at the frequency of 12GHz.

We can observe in [Annex 4.4.3.3] that there is a notable improvement in the coupler, because we have higher coupler signal S_{61} that in the other cases, with 0.9dB. This is because all the other exits of the frequency of operating are almost insignificants.

In the following graphic we present the electric field and electromagnetic field so we can visualize the good coupling.

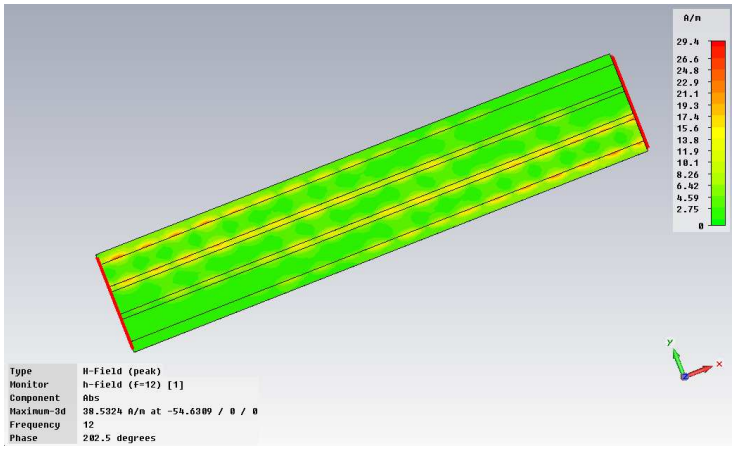

Fig. 3.19 Magnetic field of the coupled microstrip lines $(f = 12\text{GHz})$

3.5 Four coupled lines

We give some details of the simulation with four coupler lines. In this design is needed a number of eight ports, like we can see.

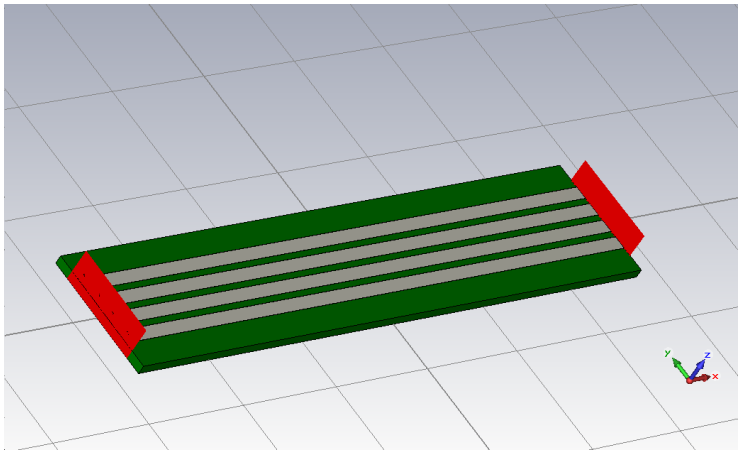

Fig. 3.20 Four coupled microstrip transmission lines.

We can see the obtained results in [Annex 4.4.4]. the design works worse that the others, has a higher difficulty of design. At the variation of the fisic parameters like we have done with the other designs, is creating some major differences between the results and we can observe distortions in the functions of parameters of the S matrix.

Bibliography

[1] S. J. Orfanidis, *"Electromagnetic Waves & Antennas"*

[2] M. Sucher and J. Fox, editors, "*Handbook of Microwave Measurements",* third edition, volume II, Polytechnic Press, New York, 1963.

[3] Ganesh Prasad Srivastava, Vijay Laxmi Gupta, *"Microwave Devices and Circuit Design"*

[4] L.Young, *" The analytical Equivalence of the TEM-Mode Directional Coupled and Transmission Line Stepped Impedance Filters"* Proc. IEEE.1963

[5] K. C. Gupta *"Microstrip lines and slotlines"* 2nd ed.

Annexes

4.1 Annex 1

4.1.1 Funtion fh

```
function dy = fh(t,y)
dy = zeros(8,1);    % a column vector
global B k X
dy(1) = B * y(2) + k * y(4) - X * y(8);
dy(2) = (X * y(7) - B * y(1) - k * y(3));
dy(3) = k * y(2) + B * y(4) - X * y(6);
dy(4) = (X * y(5) - k * y(1) - B * y(3));
dy(5) = -B * y(6) - k * y(8) + X * y(4);
dy(6) = (-X * y(3) + B * y(5) + k * y(7));
dy(7) = -k * y(6) - B * y(8) + X * y(2);
dy(8) = (-X * y(1) + k * y(5) + B * y(7));
```

4.1.2 Main funtion (Graphic 1.4)

```
[B,k,X] = soluzione1 (0.341*10^-10,1.137*10^-7,1.1367*10^-10,2.842*10^-7,1800*10^6)
L0=0; Lf=3;
Lspan=[L0 Lf];
y0=[1 0 0 0 0 0 0 0];
[l,Y] = ode23(@fh,Lspan,y0);
a1=Y(:,1)+i*Y(:,2);
a2=Y(:,3)+i*Y(:,4);
b1=Y(:,5)+i*Y(:,6);
b2=Y(:,7)+i*Y(:,8);
plot(l,a1,'-',l,a2,'-.',l,b1,'.',l,b2,'-o')
xlabel('z')
ylabel('V')
title('soluzione')
```

4.1.3 Funtion soluzione1

```
function [B,k,X] = soluzione1 (Cm,Lm,Co,Lo,f)
global B k X
B=2*pi*f*sqrt(Lo*Co);
k=1/2*B*(Lm/Lo-Cm/Co);
X=1/2*B*(Lm/Lo+Cm/Co);
```

4.2 Annex 2

4.2.1 Input parameters

```
Zo=50;
Vg1=1;
Vg2=0;

x=0:0.001:3;
Cm=0.341*10^-10;
Lm=1.137*10^-7;
Co=1.1367*10^-10;
Lo=2.842*10^-7;
f=1800*10^6;
l=0.0978;
B=2*pi*f*sqrt((Lo+Lm)*(Co-Cm));
b=2*pi*f*sqrt((Lo-Lm)*(Co+Cm));
Z=sqrt((Lo+Lm)/(Co-Cm));
z=sqrt((Lo-Lm)/(Co+Cm));
R=(Zo-Z)/(Zo+Z);
r=(Zo-z)/(Zo+z);
V=1/4*(1-R)*(Vg1+Vg2);
v=1/4*(1-r)*(Vg1-Vg2);
```

4.2.2 Main funtion (Graphic 1.5)

```
V1=((exp(-j*B*x)+R*exp(-2*j*B*l)*exp(j*B*x))/(1-R*R*exp(-2*j*B*l))*V)+((exp(-j*b*x)+r*exp(-
2*j*b*l)*exp(j*b*x))/(1-r*r*exp(-2*j*b*l))*v);
V2=(exp(-j*B*x)+R*exp(-2*j*B*l)*exp(j*B*x))/(1-R*R*exp(-2*j*B*l))*V-(exp(-j*b*x)+r*exp(-
2*j*b*l)*exp(j*b*x))/(1-r*r*exp(-2*j*b*l))*v;
plot(x,V1,'-',x,V2,'-.')
xlabel('Z')
ylabel('y')
title('soluzione')
```

4.3 Annex 3

4.3.1 Initial Value funtion

```
function [a10,a20,b10,b20]=iniziali(Cm,Lm,Co,Lo,f)
global a10 a20 b10 b20
x=0;
Zo=50;
Vg1=1;
Vg2=0;
l=0.0978;
B=2*pi*f*sqrt((Lo+Lm)*(Co-Cm));
b=2*pi*f*sqrt((Lo-Lm)*(Co+Cm));
Z=sqrt((Lo+Lm)/(Co-Cm));
z=sqrt((Lo-Lm)/(Co+Cm));
R=(Zo-Z)/(Zo+Z);
r=(Zo-z)/(Zo+z);
V=1/4*(1-R)*(Vg1+Vg2);
v=1/4*(1-r)*(Vg1-Vg2);
z0=50;

V10=((exp(-j*B*x)+R*exp(-2*j*B*l)*exp(j*B*x))/(1-R*R*exp(-2*j*B*l))*V)+((exp(-j*b*x)+r*exp(-
2*j*b*l)*exp(j*b*x))/(1-r*r*exp(-2*j*b*l))*v);
V20=(exp(-j*B*x)+R*exp(-2*j*B*l)*exp(j*B*x))/(1-R*R*exp(-2*j*B*l))*V-(exp(-j*b*x)+r*exp(-
2*j*b*l)*exp(j*b*x))/(1-r*r*exp(-2*j*b))*v;
I10=((exp(-j*B*x)-R*exp(-2*j*B*l)*exp(j*B*x))/(1-R*R*exp(-2*j*B*l))*V/Z)+((exp(-j*b*x)-r*exp(-
2*j*b*l)*exp(j*b*x))/(1-r*r*exp(-2*j*b*l))*v/z);
I20=(exp(-j*B*x)-R*exp(-2*j*B*l)*exp(j*B*x))/(1-R*R*exp(-2*j*B*l))*V/Z-(exp(-j*b*x)-r*exp(-
2*j*b*l)*exp(j*b*x))/(1-r*r*exp(-2*j*b))*v/z;
a10=(V10+z0*I10)/sqrt(2*z0);
b10=(V10-z0*I10)/sqrt(2*z0);
a20=(V20+z0*I20)/sqrt(2*z0);
b20=(V20-z0*I20)/sqrt(2*z0);
```

4.3.2 Main funtion (Graphic 1.6)

```
[a10,a20,b10,b20] = iniziali (0.341*10^-10,1.137*10^-7,1.1367*10^-10,2.842*10^-7,1800*10^6)
[B,k,X] = soluzione1 (0.341*10^-10,1.137*10^-7,1.1367*10^-10,2.842*10^-7,1800*10^6)
L0=0; Lf=3;
Lspan=[L0 Lf];
y0=[real(a10) imag(a10) real(a20) imag(a20) real(b10) imag(b10) real(b20) imag(b20)];
[T,Y] = ode23(@rigid2,Lspan,y0);
a1=Y(:,1)+i*Y(:,2);
a2=Y(:,3)+i*Y(:,4);
b1=Y(:,5)+i*Y(:,6);
b2=Y(:,7)+i*Y(:,8);
z0=50;
V1=(a1+b1)*(sqrt(z0))/sqrt(2);
V2=(a2+b2)*(sqrt(z0))/sqrt(2);
P=(((abs(a1)).^2)+((abs(a2)).^2)-((abs(b1)).^2)-((abs(b2)).^2));
plot(T,V1,'-',T,V2,'-.',T,P,'.')
xlabel('Z')
ylabel('Y')
title('soluzione')
```

4.4 Annex 4 (Simulation in CST)

4.4.1 A microstrip

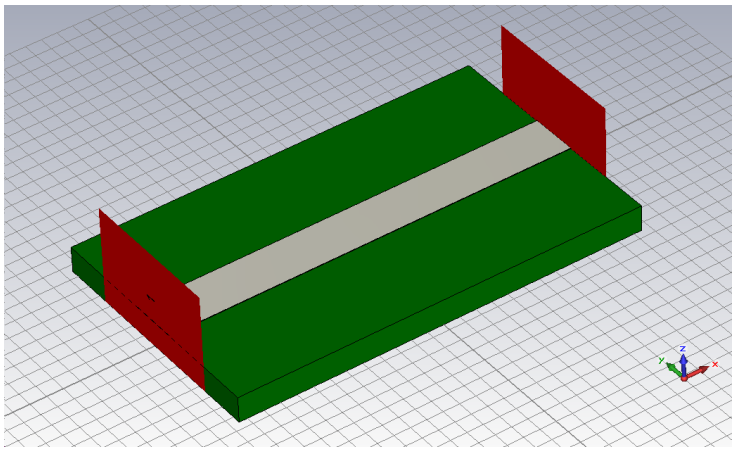

Fig. A4.1 A microstrip line in CST.

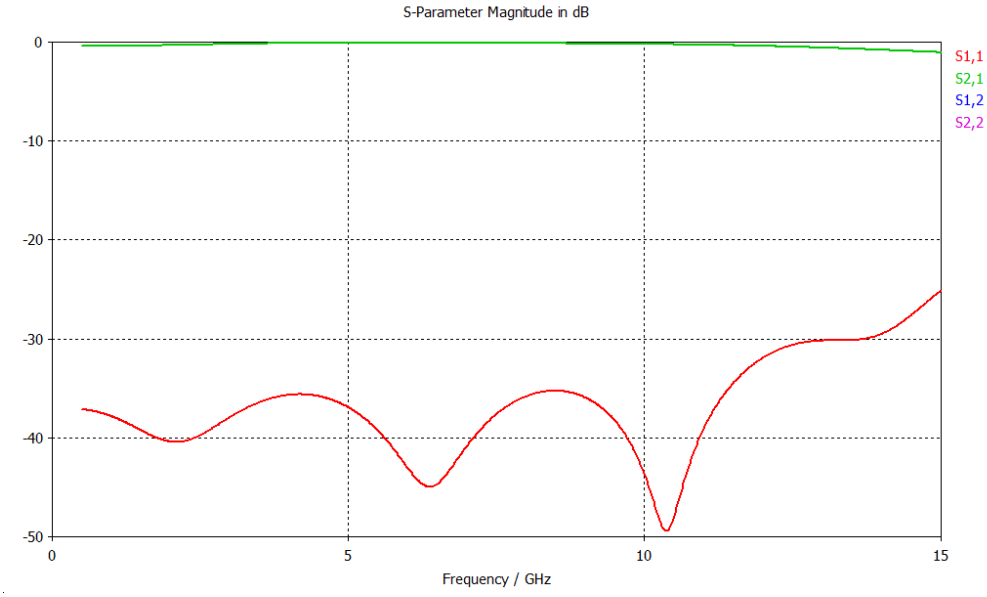

Fig. A4.2 S matrix parameters.

4.4.2 Two coupled lines

4.4.2.1 Microstrip with $W = 1.5\,h$ and $S = 0.7\,h$

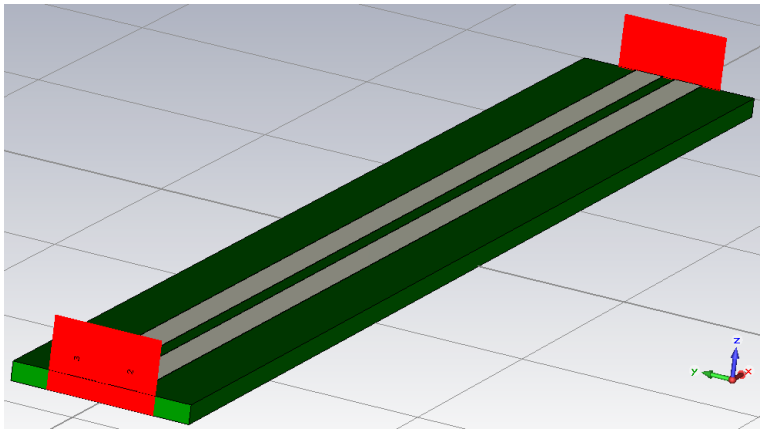

Fig. A4.3 Two coupled microstrip transmission lines with $W = 1.5\,h$ and $S = 0.7\,h$

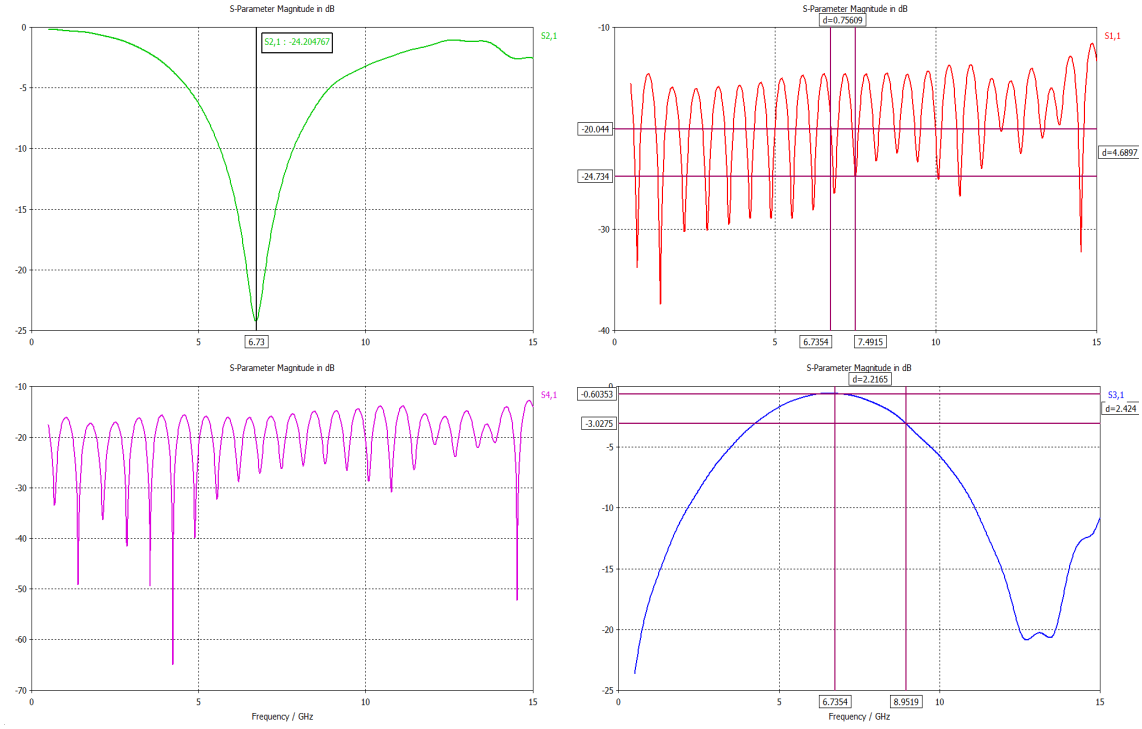

Fig. A4.4 S matrix parameters.

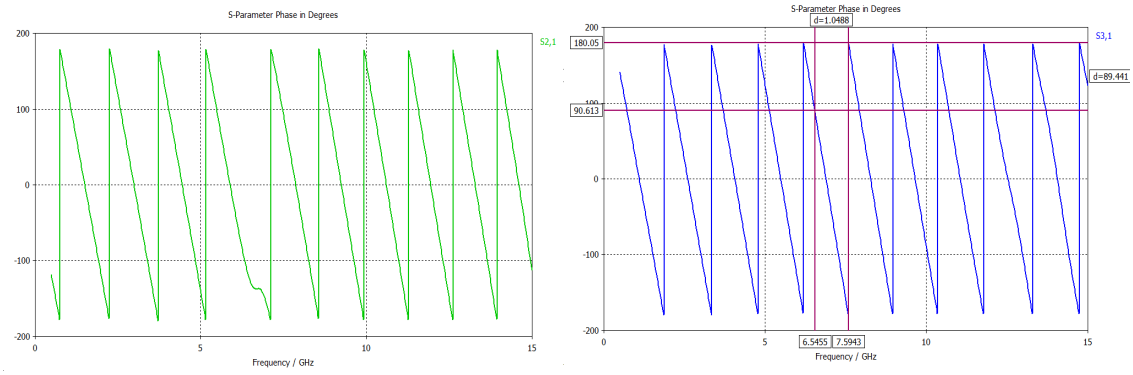

Fig. A4.5 S matrix parameters phases.

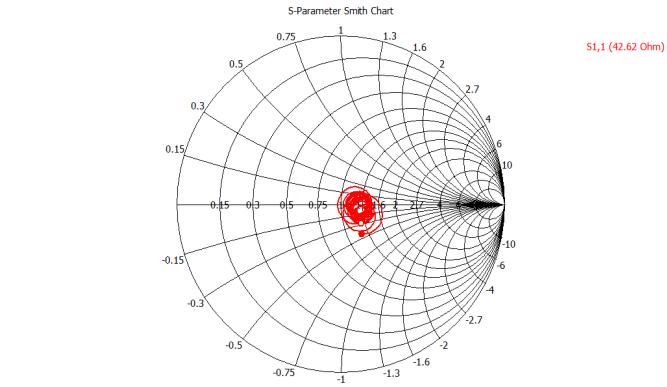

Fig. A4.6 S parameters smith chart.

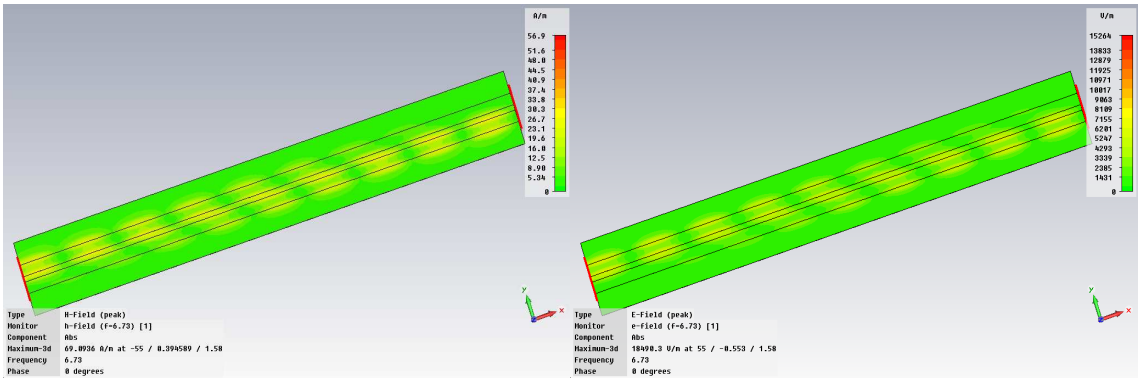

Fig. A4.7 Magnetic and electrical field of the coupled microstrip lines ($f = 6{,}73\,GHz$).

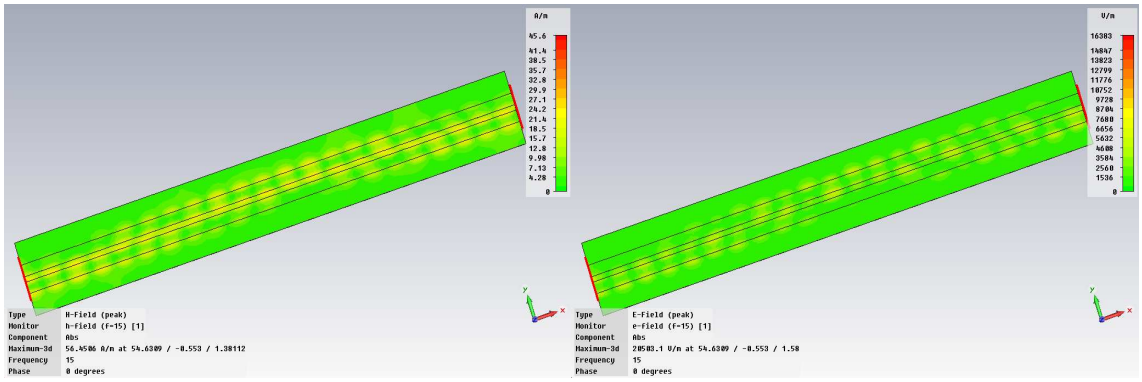

Fig. A4.8 Magnetic and electrical field of the coupled microstrip lines $(f = 15\text{GHz})$.

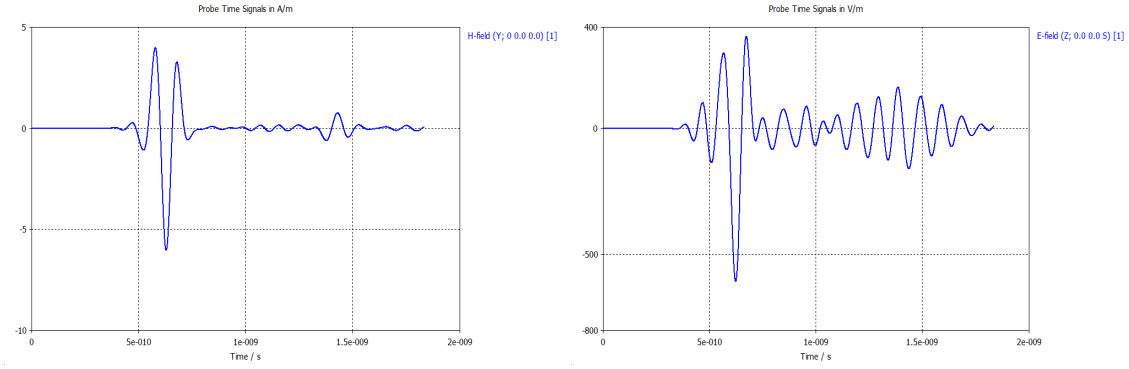

Fig. A4.9 Magnetic and electrical field of the coupled microstrip lines in a point (line 1).

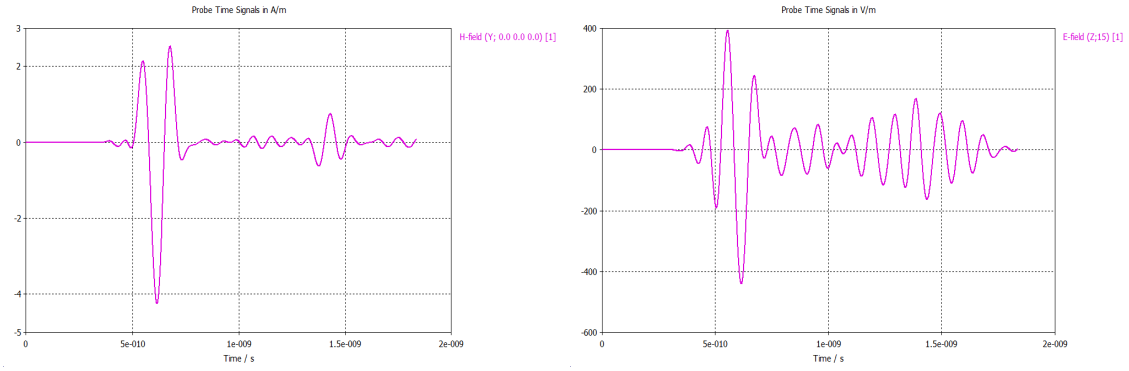

Fig. A4.10 Magnetic and electrical field of the coupled microstrip lines in a point (line 2).

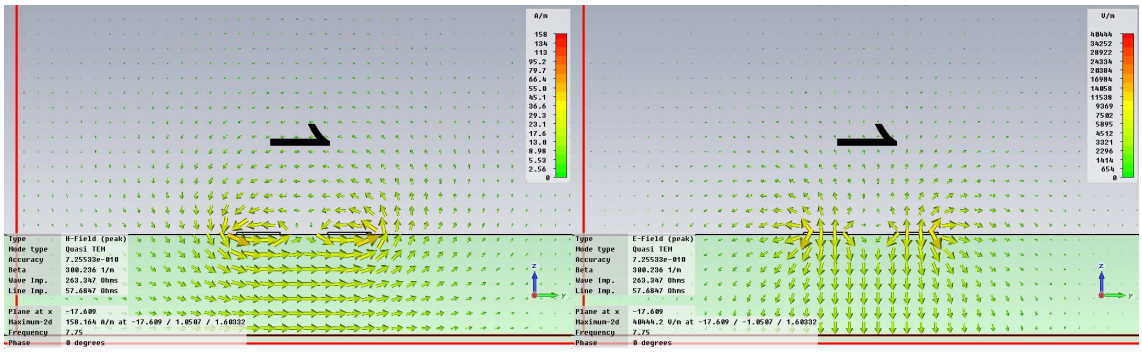

Fig. A4.11 Simulation of even mode excitations for a coupled line.

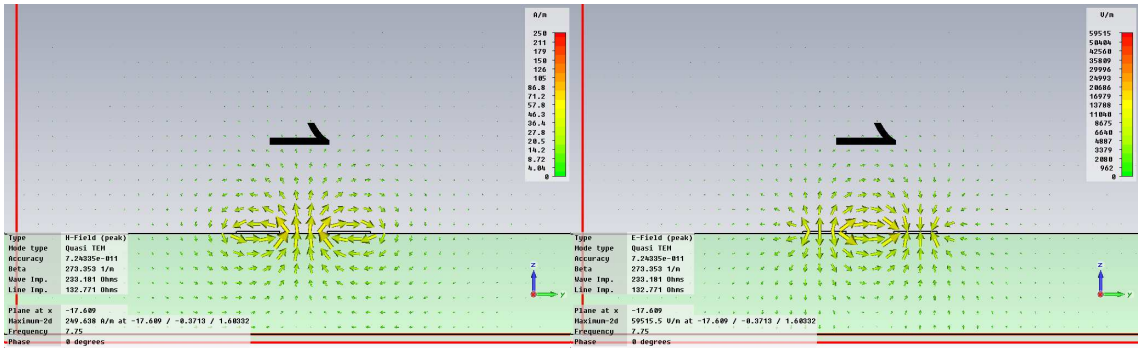

Fig. A4.12 Simulation of odd mode excitations for a coupled line.

4.4.2.2 Double length Microstrip with $W = 1.5\,h$ and $S = 0.7\,h$

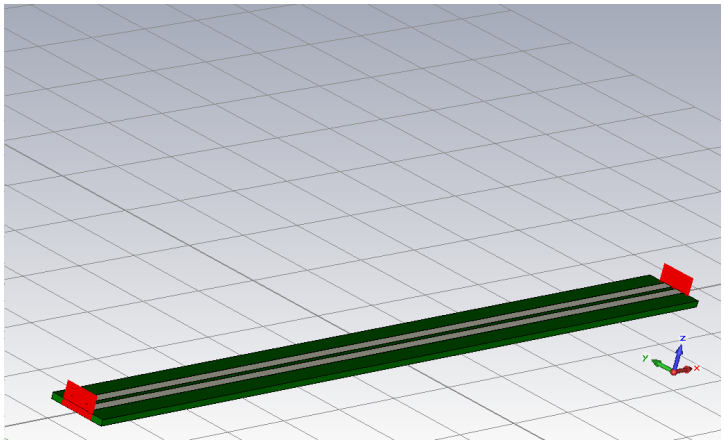

Fig. A4.13 Two coupled microstrip transmission lines with double length.

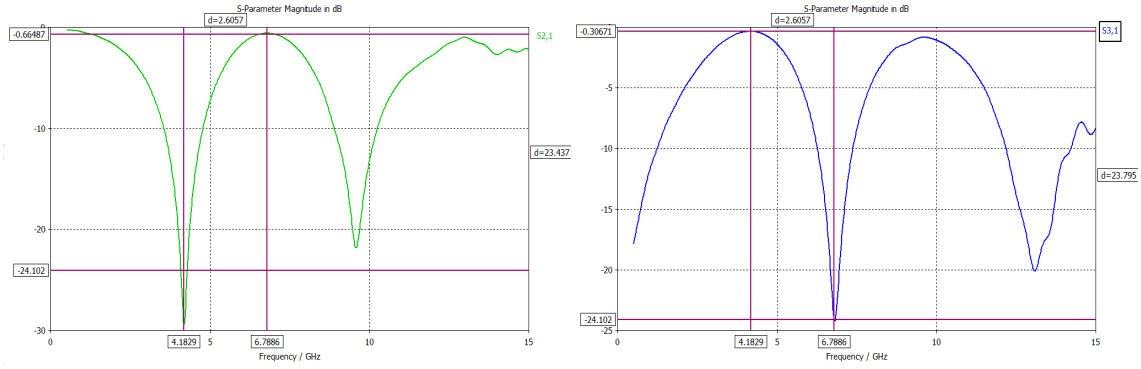

Fig. A4.14 S matrix parameters.

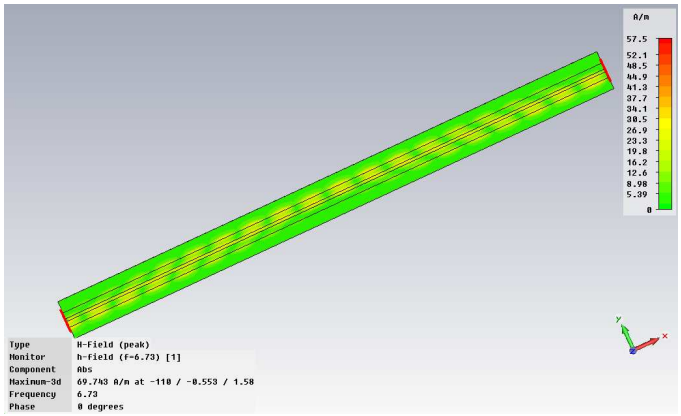

Fig. A4.15 Magnetic field of the coupled microstrip lines $(f = 6{,}73\,GHz)$.

4.4.2.3 Microstrip with $W = 1.5\,h$ and $S = 2.5\,h$

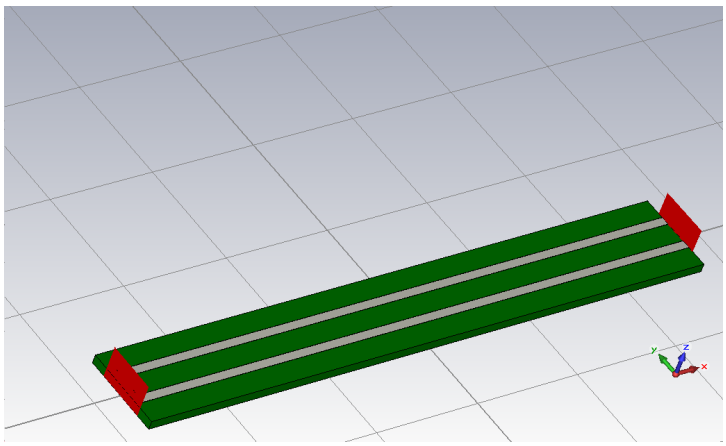

Fig. A4.16 Two coupled microstrip transmission lines.

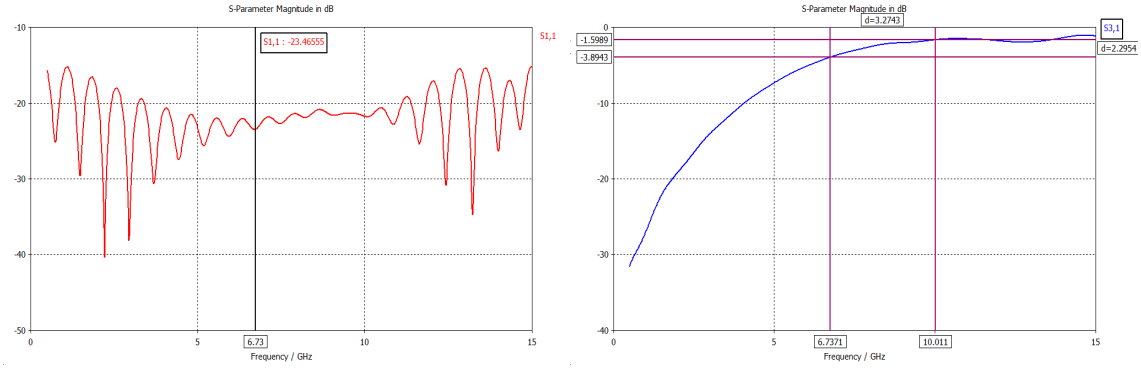

Fig. A4.17 S matrix parameters.

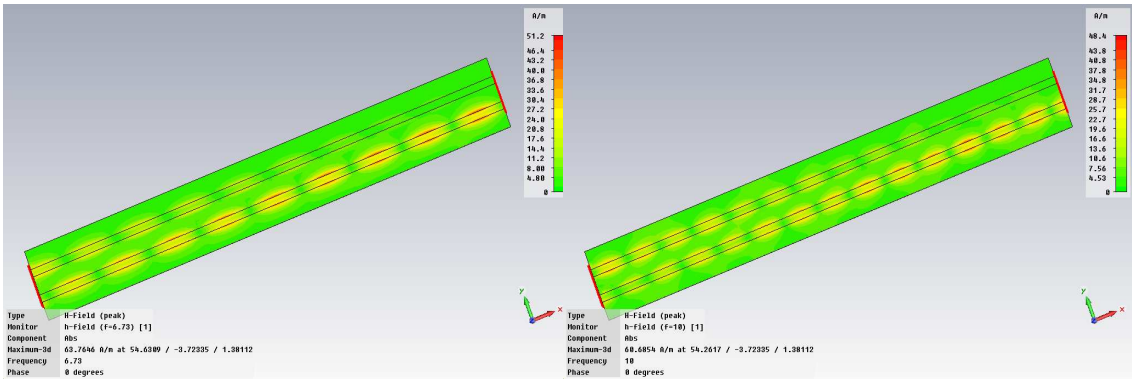

Fig. A4.18 Magnetic field of the coupled microstrip lines $(6{,}73\,GHz \wedge 10\mathrm{GHz})$

4.4.2.4 Microstrip with $W = 4\,h$ and $S = 0.7\,h$

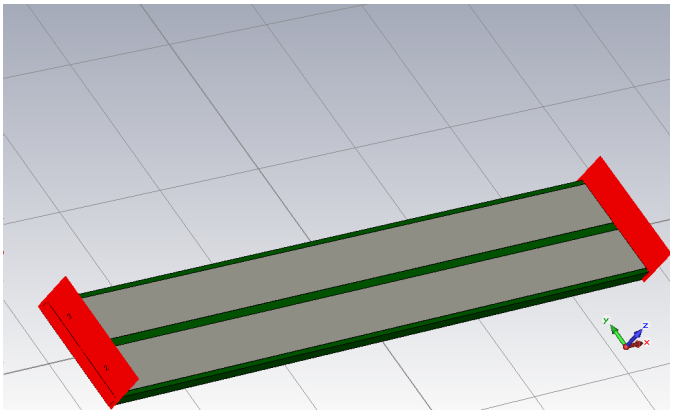

Fig. A4.19 Two coupled microstrip transmission lines.

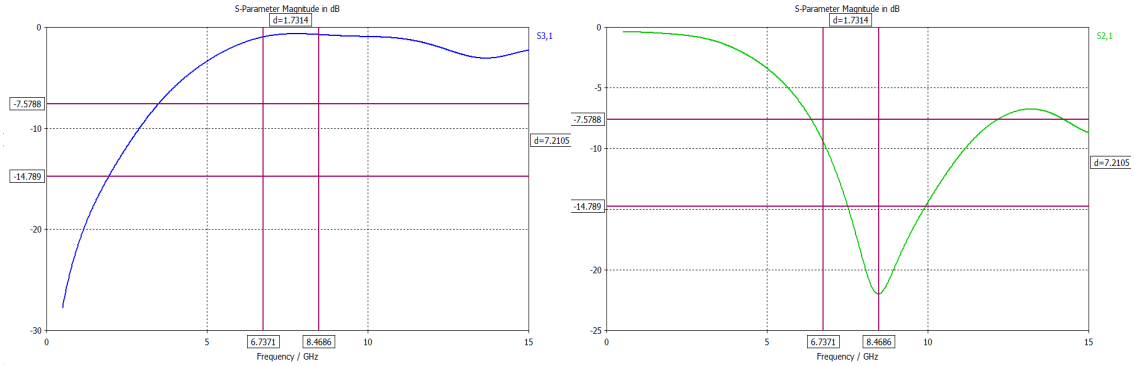

Fig. A4.20 S matrix parameters.

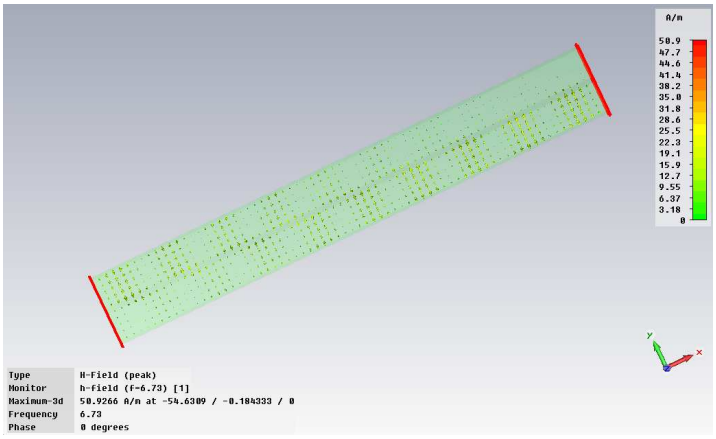

Fig. A4.21 Magnetic field arrows of the coupled microstrip lines ($f = 6{,}73\,GHz$)

4.4.3 Three coupled lines

4.4.3.1 Microstrip with $W = 1.5\,h$ and $S = 0.7\,h$

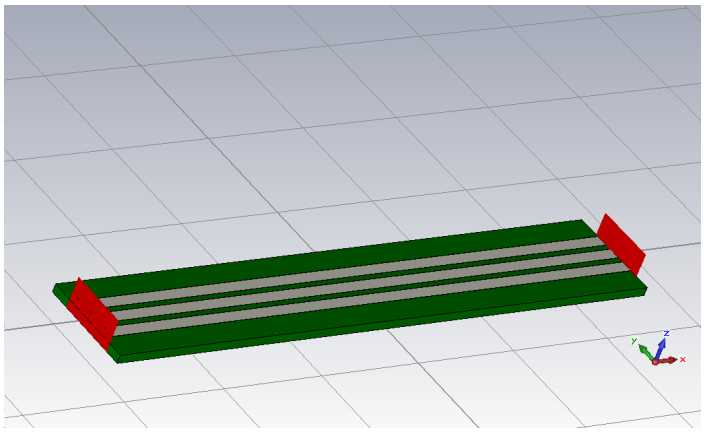

Fig. A4.22 Three coupled microstrip transmission lines.

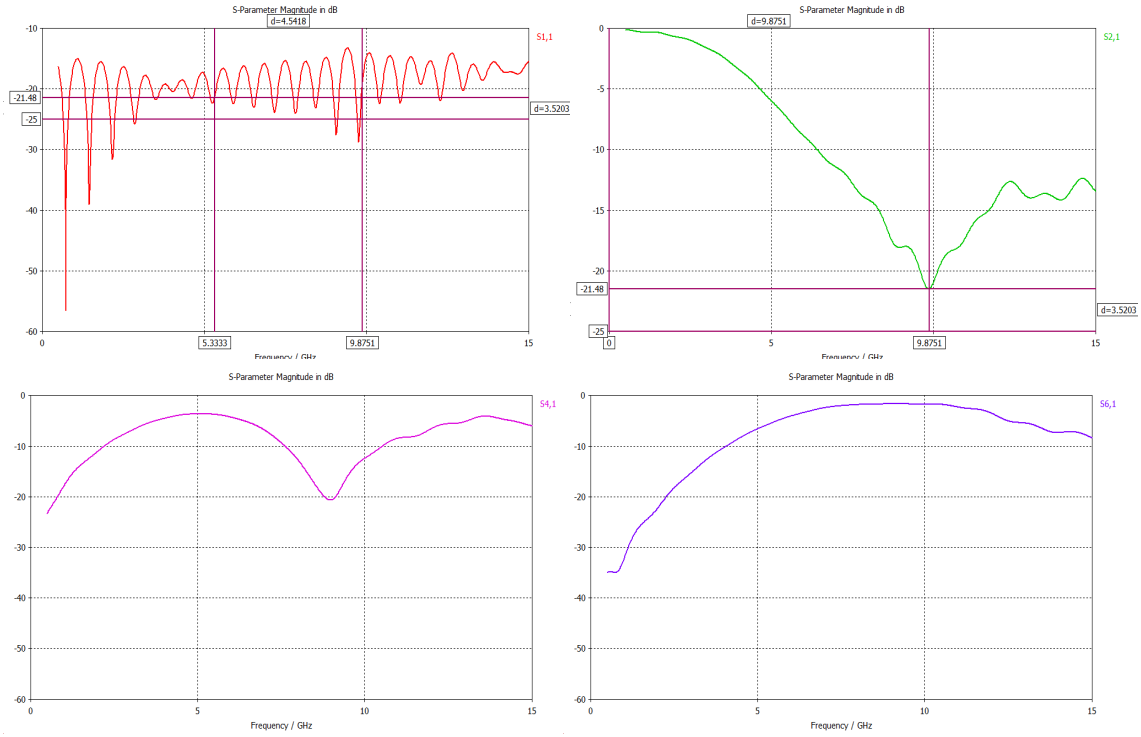

Fig. A4.23 S matrix parameters.

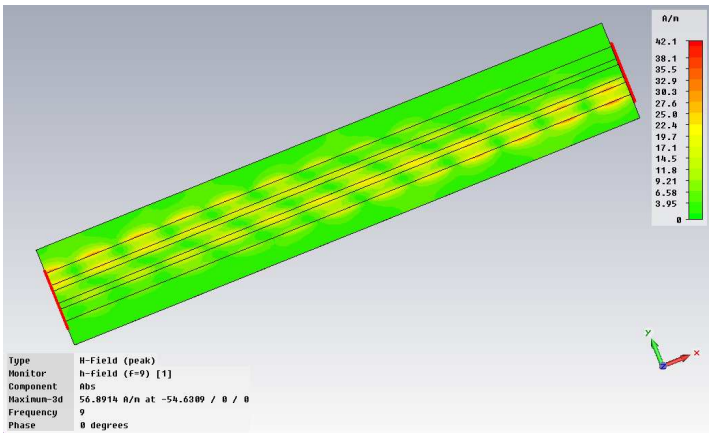

Fig. A4.24 Magnetic field of the coupled microstrip lines（$f=9\mathrm{GHz}$）

4.4.3.2 Microstrip with $W = 1.5\,h$ and $S = 4\,h$

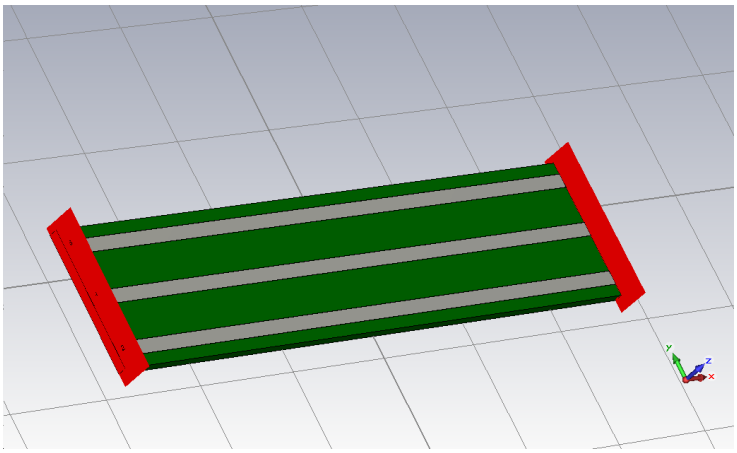

Fig. A4.25 Three coupled microstrip transmission lines.

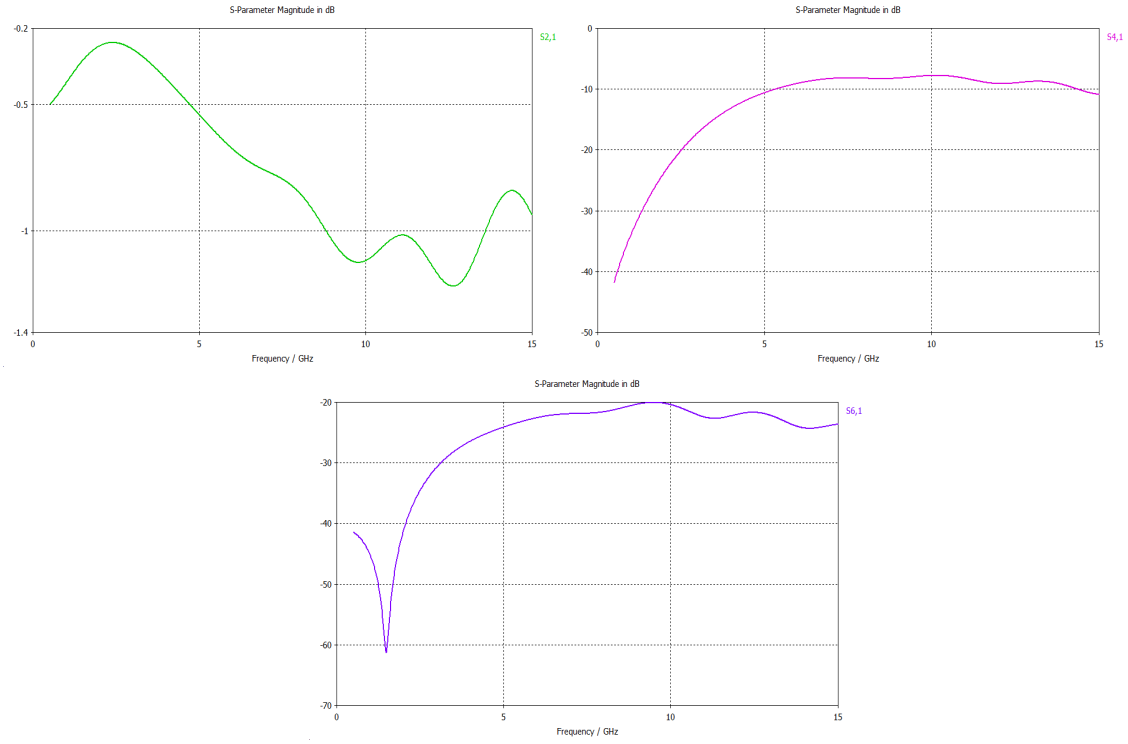

Fig. A4.26 S matrix parameters.

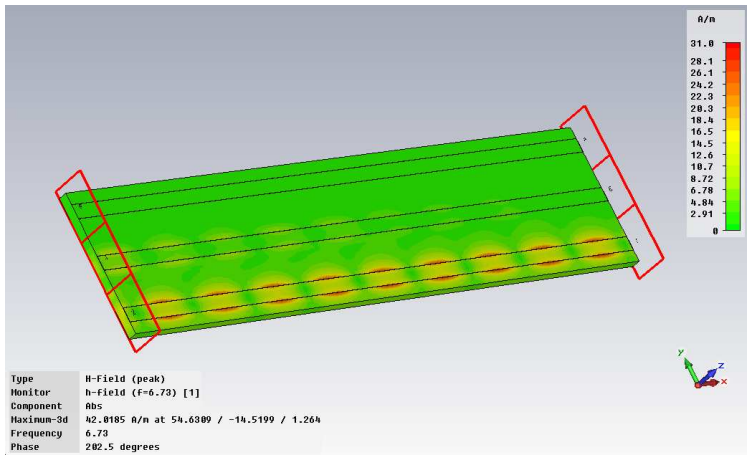

Fig. A4.27 Magnetic field of the coupled microstrip lines ($f = 6.73\text{GHz}$)

4.4.3.3 Microstrip with $W = 3h$ and $S = 0.7h$

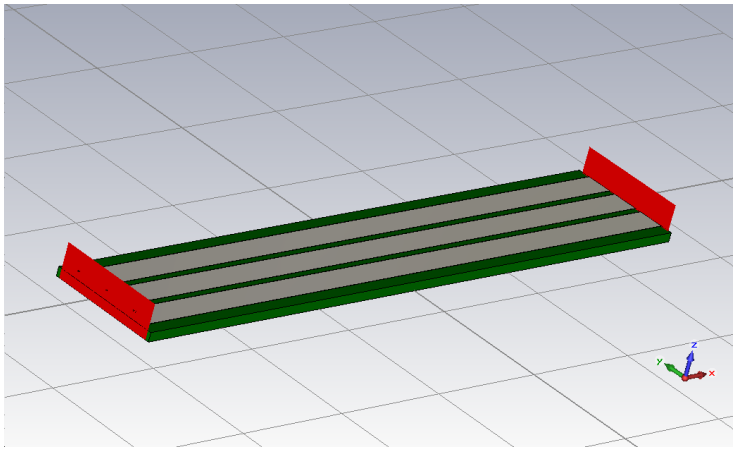

Fig. A4.28 Three coupled microstrip transmission lines.

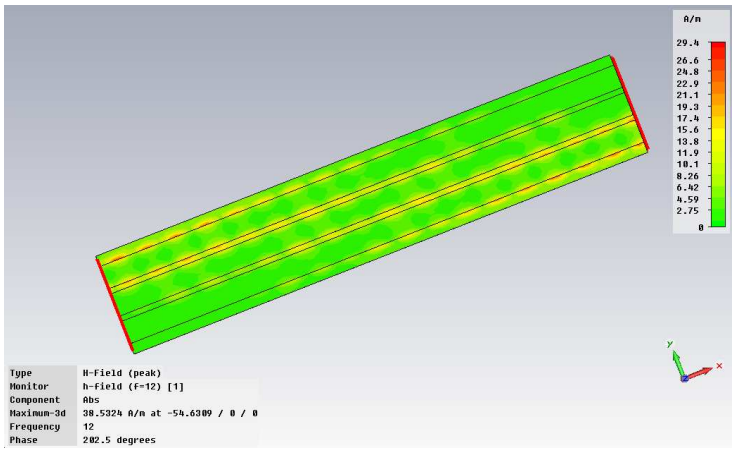

Fig. A4.29 Magnetic field of the coupled microstrip lines ($f = 12\text{GHz}$)

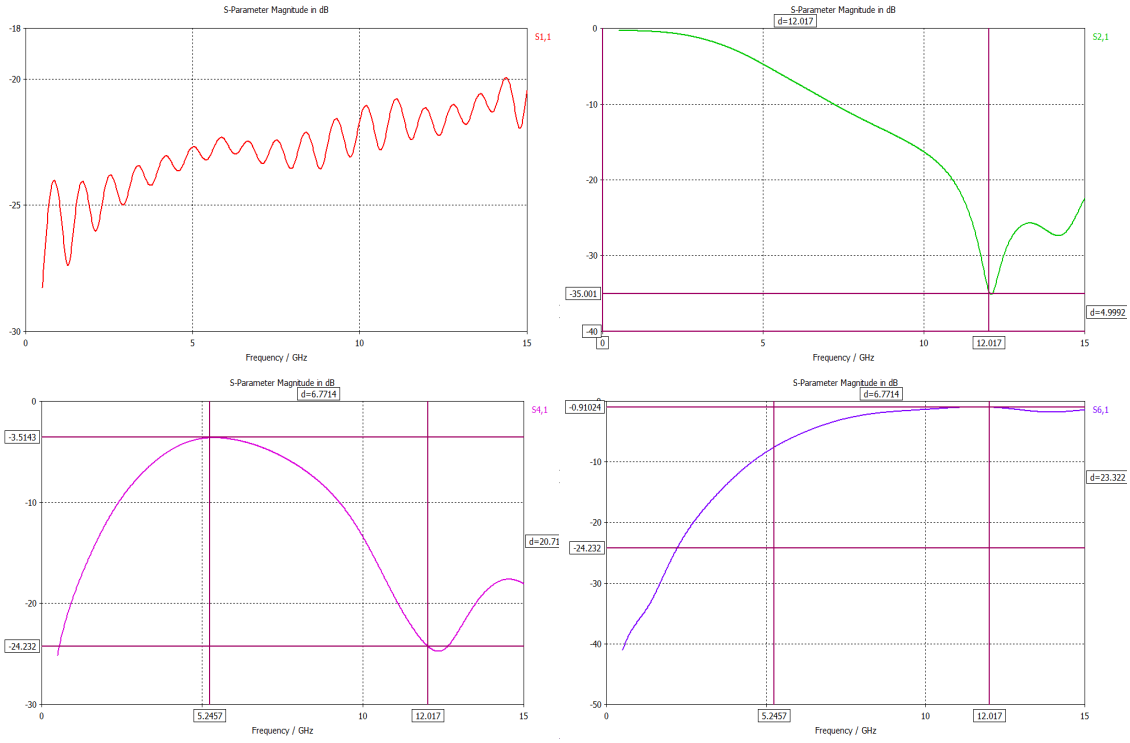

Fig. A4.30 S matrix parameters.

4.4.4 Four coupled lines

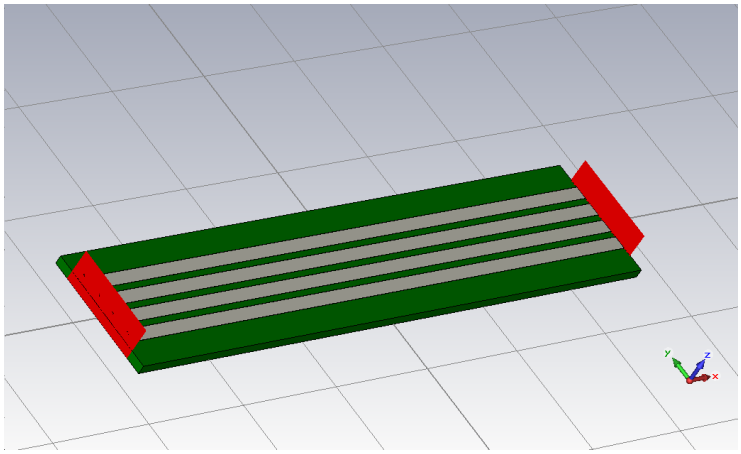

Fig. A4.31 Four coupled microstrip transmission lines.

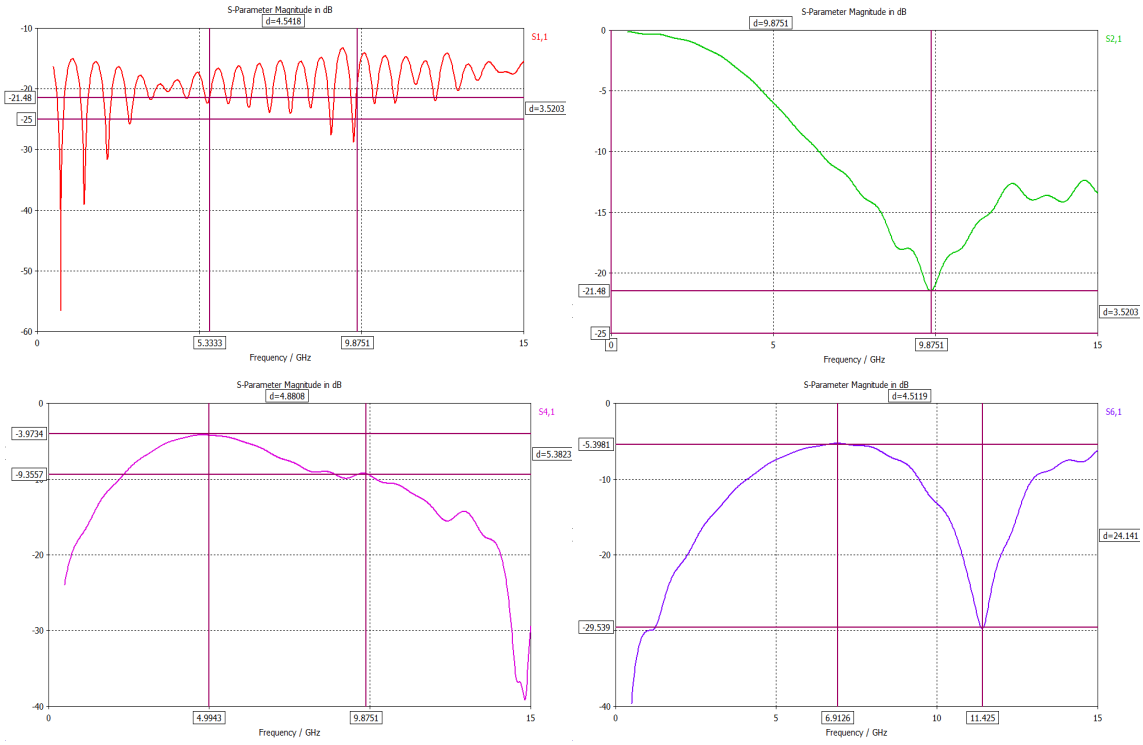

Fig. A4.32 S matrix parameters.

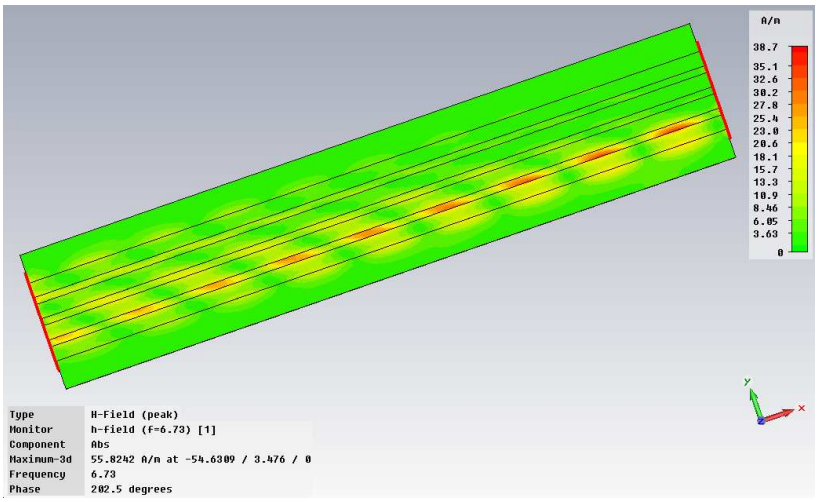

Fig. A4.33 Magnetic field of the coupled microstrip lines（f =6.73GHz）

Libraries and Documentation Service of the Technical University of Catalonia's authorization to disseminate copyrighted papers via its website

Mr. CARLOS SANCHEZ SIERRA, with passport number 44420474E, author of the paper titled "MICROWAVE DIRECTIONAL COUPLERS", authorizes the Libraries and Documentation Service of the Technical University of Catalonia the dissemination of his/her paper according to the following conditions:

1. Make electronically available the aforementioned paper by including it on the website of the Libraries and Documentation Service of the Technical University of Catalonia or any other platform that may take its place.

2. Adapt the paper, when technically necessary, in order to make it electronically available via the website.

3. The undersigned grants the dissemination of the paper:

[Mark the chosen option]

( ) through the *Attribution-Noncommercial-Share Alike* Creative Commons license or similar
[You let others copy, distribute, transmit and adapt your paper. You allow others to distribute derivative papers only under a license identical to the license that governs your paper]

( ) through the *Attribution-Non-commercial-No Derivative Works* Creative Commons license or similar
[You let others copy, distribute and transmit only verbatim copies of your paper, not derivative papers based on it].

These licenses grant, in all cases, the authority to reproduce, distribute, and disseminate the paper by any person as long as authorship is acknowledged, and for non-commercial purposes only.

(X) without any Creative Commons license or similar granted

This agreement by no means signifies an exclusive assignment of author copyright to the paper, nor does it prevent typical forms of commercialization.

This agreement is valid for a period of 5 years, which can be automatically extended for successive periods of the same length, except in the case in which the agreement is expressly repealed by the author of the paper.

I hereby state that I am the legitimate owner of the copyright to the paper here discussed, and have obtained the necessary permission to include in it other papers of which I am not the author (photographs, drawings, texts, etc.).

BRESCIA, 16 of July of 2010

The Author

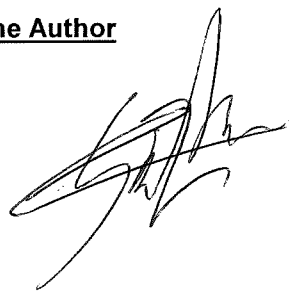

Supervisor Agreement